POLITECNICO DI TORINO

Dipartimento di Ingegneria dell'Ambiente, del Territorio e delle Infrastrutture

Master of Science Course
in Environmental Engineering, Natural Hazard and Civil Protection

Master of Science Thesis

Avalanche dynamics and its impact on transport infrastructure: A case study of the Podljubelj Avalanche Tunnel, Slovenia.

Tutors
Barbara Frigo
Blaž Komac

Candidate
Mattia Matzutzi

March 2025

TABLE OF CONTENTS

1. Abstract

This thesis begins with a comprehensive analysis of the avalanche phenomenon. Following a general overview, the study examines the snowpack, avalanche classification, and the modelling methodologies employed to analyse avalanche dynamics, with a particular focus on the RAMMS Avalanche software. The first section also includes an overview of protective structures and risk mitigation strategies, providing an in-depth examination of the impact forces exerted by avalanches on structures, with special attention to the effects on avalanche protection tunnels.

The thesis then proceeds with an analysis of avalanche interference with the Podljubelj tunnel (SLO), which presents critical issues under conditions of multiple avalanche events. The case study is introduced through a description of the geographical context, the avalanche site, and the tunnel structure itself. The investigation continues with a historical analysis of past avalanche events to define release areas and snow depths—key input parameters for the RAMMS software. Where data were unavailable, values were estimated based on climatic and snowpack analyses.

To identify critical conditions for the tunnel (i.e., scenarios in which one or more avalanche events obstruct the road and block tunnel entrances), the RAMMS software (developed by SLF, Davos, CH) was used to analyse avalanche dynamics and define critical scenarios and release conditions. Following an in-depth assessment of the avalanche basin and the dynamic characteristics of the avalanche events—necessary for calibrating the software for the specific study area—several dynamic simulations were performed, varying only the release snow depth (and consequently, the overall snowpack height). Each defined scenario provides an estimate of the avalanche runout distance and the potential interference with the road and tunnel.

Furthermore, the thesis evaluates the impact of multiple avalanche events, including those of smaller magnitude, whose dynamics may become anomalous due to the presence of previous snow deposits near or above the tunnel. In addition to assessing the effectiveness of the existing protective structure (the tunnel), this dynamic analysis provides essential data—such as the critical snowpack height at the release zone, related to the release thickness—for road risk management.

The final section of the thesis presents a road avalanche risk assessment, considering the presence of the protective tunnel. This includes an estimation of the probability of a vehicle being blocked by an avalanche, the risk of fatality, and rear-end collision risks based on real winter traffic data. Finally, in the context of a potential tunnel extension to mitigate critical avalanche interferences, the study compares the construction costs of permanent infrastructure solutions (avalanche protection tunnels) across various European countries. As will be discussed, from an economic perspective, such solutions may not always be the optimal choice.

La presente tesi si apre con un'analisi approfondita del fenomeno delle valanghe. Dopo una panoramica generale, vengono esaminati il manto nevoso, la classificazione delle valanghe e le metodologie di modellazione impiegate per studiarne la dinamica, con un focus sul software RAMMS Avalanche. La prima parte include anche una panoramica sulle opere di difesa e sulle strategie di mitigazione del rischio valanghivo, con un'analisi approfondita delle forze d'impatto esercitate dalle valanghe sulle strutture, ponendo particolare attenzione agli effetti sui tunnel antivalanga.

La tesi prosegue con l'analisi dello studio dell'interferenza valanghiva con il tunnel di Podljubelj (SLO) che presenta delle criticità in condizioni di eventi valanghivi multipli. Il caso studio viene introdotto attraverso una descrizione del contesto geografico, del sito valanghivo e della struttura stessa. L'indagine prosegue con l'analisi storica degli eventi valanghivi al fine della definizione delle aree e dello spessore di distacco, input principali del software RAMMS. Per quest'ultimo, laddove i dati sono risultati assenti, i valori sono stati stimati grazie ai dati ottenuti dalle analisi climatiche e nivologiche.

Al fine dell'individuazione delle condizioni di criticità per il tunnel (ovvero le situazioni in cui il singolo o più eventi invadono la strada ostruendo gli ingressi del tunnel), si è utilizzato il software RAMMS (del SLF di Davos, CH) per l'analisi della dinamica valanghiva e per la definizione degli scenari (e condizioni di distacco) critici. Dopo l'analisi dello specifico bacino valanghivo e delle caratteristiche dinamiche degli eventi valanghivi, ovvero la taratura del software per il bacino stesso, vengono condotte varie simulazioni dinamiche, variando esclusivamente lo spessore di distacco (e, pertanto la relativa altezza del manto nevoso). Ogni scenario definito fornisce una stima della distanza d'arresto e sulla possibile interferenza con la strada e con il tunnel.

La tesi valuta inoltre l'effetto di eventuali eventi multipli, ovvero valanghe di magnitudo anche minori, ma con distacchi che possono mostrare delle dinamiche anomale a causa dei precedenti depositi a ridosso o al di sopra del tunnel. Oltre alla verifica dell'efficienza dell'opera di difesa realizzata (tunnel), questa analisi dinamica fornisce inoltre elementi essenziali (l'altezza critica del manto nevoso in zona di distacco, legata allo spessore di distacco) per la gestione del rischio su strada.

La parte conclusiva della tesi presenta l'analisi di rischio valanghe su strada, considerando la presenza dell'opera di difesa (tunnel). Viene, perciò, stimata la probabilità che un veicolo venga bloccato da una valanga, il rischio di mortalità e di tamponamento in base ai dati reali dei passaggi invernali. Nell'ipotesi di un prolungamento del tunnel per ovviare alle interferenze valanghive critiche, vengono, infine, confrontati i costi di realizzazione di soluzioni infrastrutturali permanenti (i tunnel antivalanga) in diversi paesi europei che, come si vedrà, dal punto di vista economico, potrebbero non essere sempre la scelta ottimale

2. Avalanche Definition

Avalanches represent a significant natural hazard, particularly in the Alps, where the high population density in mountainous valleys increases the exposure of buildings and infrastructure to avalanche-related risks. This study focuses exclusively on snow avalanches; for simplicity, the term "avalanche" will hereafter refer solely to snow-related phenomena. An avalanche is the downslope movement of a mass of snow under the influence of gravity. The European Avalanche Warning Services (EAWS) define an avalanche as the rapid movement of a snow mass with a volume exceeding 100 m^3 and a total length greater than 50 meters (www.avalanches.org). The total length of an avalanche is measured from the highest point of the fracture to the farthest point of the deposit. For smaller volumes and shorter runout distances, it is more appropriate to refer to snow flows or sluff releases (Frigo, 2003), while the term *"slavina"* is not scientifically accurate (Pagnutti & Della Santa, 2004).

In the starting zone (Figure 2.1), the primary topographic factor influencing the triggering of an avalanche is the slope angle, which facilitates the initiation and acceleration of the avalanche phenomenon. Potential release areas are typically confined to terrains with angles between 30° and 50° because slopes exceeding 50° tend to produce frequent, small avalanches due to limited snow deposition, whereas angles below 30° lack sufficient gravitational force to initiate avalanches (Maggioni & Gruber 2003, Komac et al, 2023).

A second critical element is wind, due to its multifaceted influence on snowpack dynamics. It redistributes snow, leading to localized overloading on slopes and increasing the likelihood of release. Wind-driven compaction can form unstable slabs over weak snow layers. Furthermore, wind erosion reduces snowpack thickness, creating areas of weakness. The direct pressure exerted by wind adds stress to the snow cover, while also affecting snow metamorphism, potentially leading to the formation of fragile crystals that destabilize the snowpack. Studies in the Davos area reveal a direct correlation between avalanche activity and strong winds in over 40% of recorded events. Wind-transported snow contributes additional loads to leeward areas, with wind speed, direction, and precipitation rates all impacting avalanche prediction models (Meister, 1989).

Additionally, the exposure of slopes to solar radiation plays a significant role, as it influences snowpack stability by contributing to radiation recrystallization, a process that can lead to the formation of weak layers due to the balance between incoming solar heat and outgoing longwave radiation losses. This phenomenon creates a thermal gradient that promotes the development of melt-freeze facets, particularly on south-facing slopes. If preserved by subsequent snowfall, these weak layers can act as sliding surfaces and trigger avalanche cycles (Kelly & Staples 2023).

Vegetation exerts a complex stabilizing influence on the snowpack: trees mitigate the deposition of substantial quantities of wind-transported snow, intercept and gradually release snow from their branches, and serve as physical barriers due to their trunks. Specifically, a crown coverage exceeding 30% and the absence of gaps longer than 25 meters diminish the likelihood of avalanche

release. Conversely, shrubs can negatively affect stability by disrupting the formation of a homogeneous snowpack and fostering the development of weak, poorly bonded layers. It is crucial to acknowledge that the efficacy of trees in preventing avalanche formation is contingent upon specific conditions; for instance, their capacity to intercept snow is mediated by tree species and prevailing meteorological conditions during snowfall. Furthermore, snowpack properties can undergo abrupt alterations due to natural disturbances or anthropogenic interventions such as fire, windthrow, or logging, which may transiently elevate avalanche risk if woody debris is removed or decomposes (Bebi et al., 2009).

Between the start zone and the runout lies the track, also referred to as the avalanche path. The start zone is typically located near ridge crests, above the forest vegetation line, where snow accumulates due to precipitation and wind transport. This area is characterized by specific slope inclinations and internal snowpack dynamics that may lead to instability. Factors such as snow layer movements, loss of cohesion, overloads, and vibrations can trigger the failure of the snowpack along a weak layer or an interface between layers, initiating an avalanche. (Chiaia & Frigo, 2024).

As the avalanche moves downslope, it enters the track, the transition zone between the start zone and the runout. The track can take the form of either confined channels (gullies) or open slopes, leading to complex flow geometries. The absence or alteration of vegetation, such as younger trees or species differing from those in the surrounding areas, often indicates frequent avalanche activity in this zone. During an avalanche's course, a crucial phenomenon influencing its dynamics is entrainment, which involves the incorporation of snow and air. This process primarily occurs through two mechanisms: erosion and air entrainment. Erosion involves the incorporation of snow from the underlying snowpack, increasing the total mass of the avalanche and intensifying its velocity. This sustenance mechanism allows the avalanche to maintain and increase its energy during descent. Simultaneously, air entrainment lifts the powdery portion of the avalanche, modifying the overall density and increasing turbulence within the snow cloud. Thus, entrainment is a dynamic process that significantly contributes to an avalanche's mass, speed, and flow rate, influencing its behaviour and ability to propagate downstream (Gauer, 2014).

Finally, in the runout, the avalanche decelerates due to a decrease in slope inclination, typically below 15° (McClung & Schaerer, 2006), leading to snow deposition. This zone is often situated on valley floors but may also extend to broad plateaus or the opposing valley slope, depending on the terrain and flow dynamics (Chiaia & Frigo, 2024).

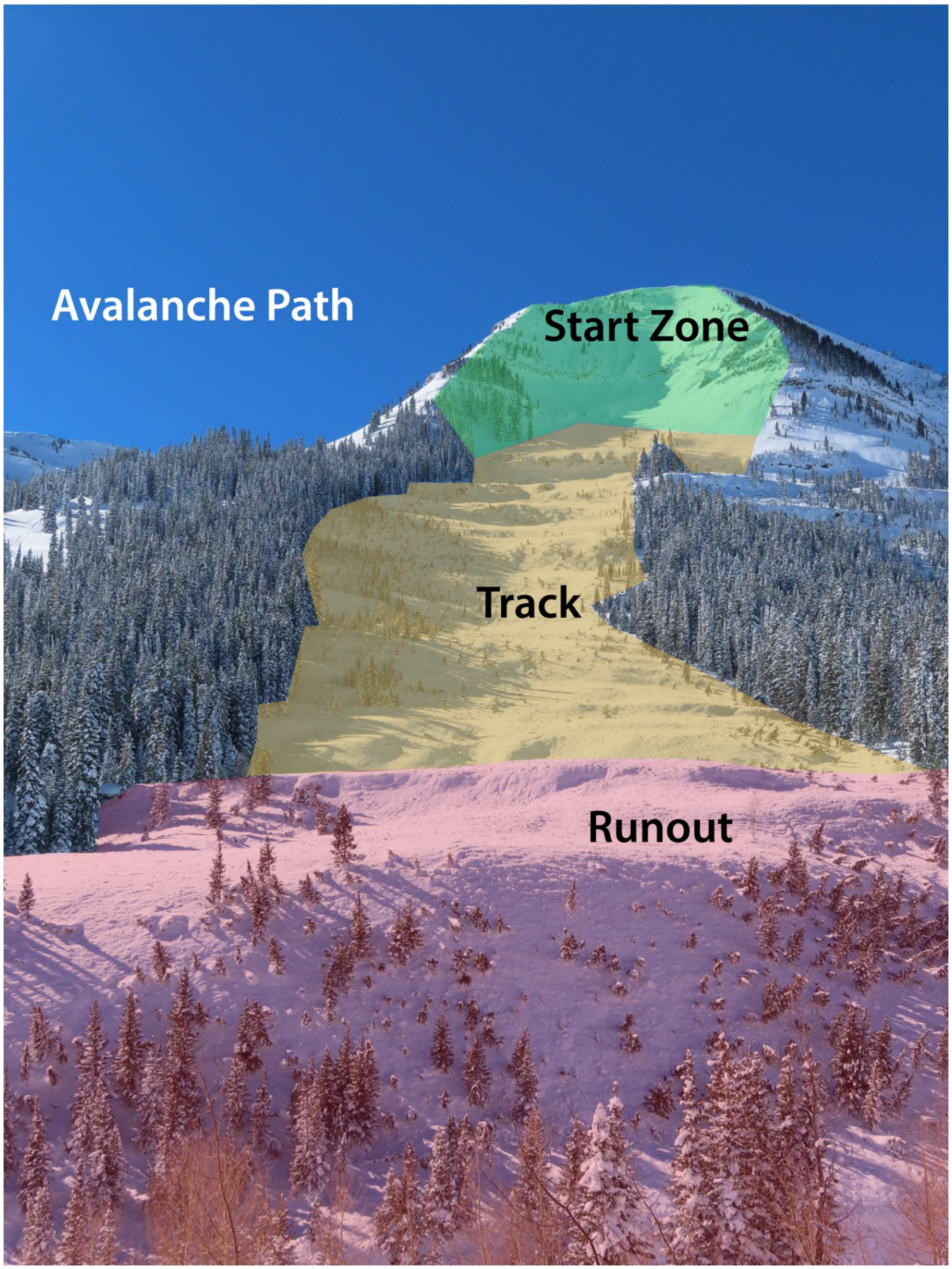

Figure 2-1 Avalanche Path (Source: www.avalanche.org, Credit: Crested Butte Avalanche Center)

2.1 Snowpack

The snowpack results from the deposition of all snow crystals formed in the atmosphere and precipitated under the influence of gravity (Praolini et al., 2005). Understanding the stability of the snowpack is crucial for preventing and mitigating natural risks in mountainous regions, although this remains a complex process due to the internal variability of the snowpack (Langham, 1992). The snowpack is a complex system composed of overlapping layers of snow, whose physical and mechanical properties vary over time and space due to meteorological and morphological factors. The stability of the snowpack is determined by the balance between internal and external forces; when this equilibrium is disrupted, an avalanche is triggered.

The primary factors influencing snowpack stability can be categorized as direct (intrinsic) and indirect (external). Direct factors include friction between layers, spatial and temporal variability in the mechanical properties of the snow, and the presence of weak layers. Indirect factors, on the other hand, encompass natural overloads (e.g., new snowfall, wind deposition, rain), artificial loads (e.g., skiers, snow grooming machines), and thermal effects, such as sudden temperature increases (Frigo et al., 2012).

The snowpack can undergo various types of deformation, including compression, tension, and shear (Figure 2.2).

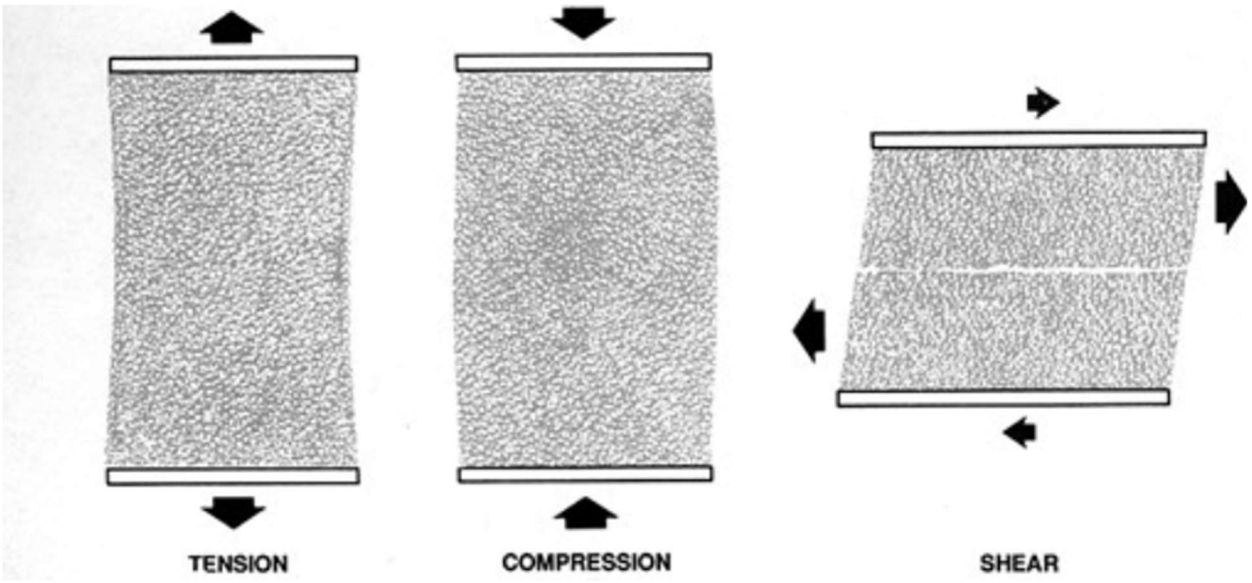

Figure 2.2 The three types of snow deformation (McClung & Schaerer, 1953)

Compression occurs when snow crystals compact, while tension manifests when snow crystals tend to separate. Compression and tension forces largely depend on the topography of the slope. When the snowpack transitions from a steep slope to a gentler one, the upper layers compress to adjust to the new inclination. Conversely, when transitioning from a gentler slope to a steeper one, the snow tends to separate, generating tension in its upper layers. Shear, on the other hand, involves the sliding of snow layers and is typically the primary cause of avalanche release. This occurs when the applied force exceeds the snowpack's shear strength. The rate of deformation is also a critical factor: if it is too slow, detachment may not occur (McClung & Schaerer, 2006). The snowpack exhibits relatively high resistance to compression but significantly lower resistance

to tension and shear (Praolini et al., 2005).

The snowpack undergoes slow, continuous movements that result in characteristic deformations, including settlement, creep, and glide. These processes are primarily governed by gravitational forces, snowpack structure, and external environmental conditions.

Settlement (compressive deformation) occurs as the snowpack gradually adjusts to external influences such as temperature fluctuations and solar radiation. This process is mainly driven by gravity, causing air to escape from the snow layers, thereby increasing density and reducing overall thickness (McClung & Schaerer, 2006).

A crucial factor preventing the snowpack from uncontrolled movement on an inclined slope is its internal cohesion and bonding to the substrate. When stability conditions are maintained, the snowpack remains anchored to the slope, with movements limited to internal shear deformations known as creep. Creep occurs due to the constant action of gravity, which induces slow, plastic deformation within the snowpack. This process is particularly pronounced on steeper slopes and in areas with a thicker snow cover, where shear stress exceeds the snow's yield strength but remains below the critical threshold for fracture (McClung & Schaerer, 2006).

By contrast, glide involves the entire snowpack and occurs at the interface between the snow and the ground. Unlike creep, which is a slow internal deformation, glide can result in sudden, large-scale snowpack displacement, significantly increasing avalanche risk (Schweizer et al., 2003).

By analysing the weight force acting on the snowpack, it is possible to decompose it into two main components that explain the snowpack's behaviour on a slope. The perpendicular component contributes to the snowpack's settlement, while the parallel component drives downslope movement. The stability of the snowpack is maintained if the downslope component of gravitational force does not exceed its shear strength. If this balance is disrupted, the snowpack may begin to slide downslope, potentially leading to an avalanche. Shear strength is primarily governed by friction at the snow-ground interface and the cohesion between snow grains within the snowpack (McClung & Schaerer, 2006). However, the presence of multiple layers within the snowpack, each with distinct physical and mechanical properties, complicates this equilibrium. Variations in density, grain size, and metamorphic processes can create weak layers, which significantly reduce overall shear strength and increase the likelihood of failure (Schweizer et al., 2003). These weak layers, often buried beneath stronger, cohesive slabs, are particularly prone to failure when subjected to additional loads or temperature fluctuations, further destabilizing the snowpack (Schweizer, 1999).

The stability (S) of the snowpack can be evaluated using an index that relates the shear force (T) to the shear resistance (R_t) of the snowpack, expressed by the formula:

$$S = \frac{R_t}{T}$$

If $R_t > T \ (S > 1)$, the snowpack is stable. If $R_t < T \ (S < 1)$, the snowpack becomes unstable. A precarious equilibrium occurs when $R_t = T \ (S = 1)$.

Instability within the snowpack can arise due to two primary factors: the presence of weak layers that reduce the snowpack's shear resistance (Rt) or an increase in shear forces, such as those generated by a skier, which enhance the applied stress (T). The occurrence of a rupture in the snowpack, leading to an avalanche, is a result of the interaction between these factors (Praolini et al., 2005). Additionally, the total depth of snow accumulation, in conjunction with the slope's inclination, plays a crucial role in determining the likelihood of instability. As the snow depth increases, the weight of the snowpack also rises, and this exacerbates the shear forces acting on the weak layers, especially on steeper slopes. Therefore, deeper snowpacks, particularly on slopes with an inclination exceeding the critical threshold (typically 30-35°), are more prone to failure (Schweizer et al., 2003). The slope angle influences the gravitational component of the force, which, when combined with the snowpack's depth, can further amplify the stress exerted on the weak layers, increasing the risk of avalanche release (McClung & Schaerer, 2006).

The surface characteristics of the snowpack are often assessed visually without the aid of measurement instruments (McClung & Schaerer, 2006). However, it is crucial to understand that the current snowpack surface can undergo transformations due to both internal and external factors, affecting its stability over time. Internal processes include snow metamorphism, changes in snow crystal structure, and variations in layering (Schweizer et al., 2003). Simultaneously, external factors such as temperature fluctuations, solar radiation, precipitation, and wind play a significant role in modifying the cohesion and structure of the snowpack (Colbeck, 1982).

When an compromised snowpack surface becomes buried by new snowfall, it can develop into a weak layer, increasing the likelihood of avalanche release (Jamieson & Schweizer, 2000). Therefore, identifying and analysing the properties of the snowpack surface before new snowfall occurs is essential for predicting potential instabilities and mitigating avalanche risk.

To characterize the snowpack's surface, it is necessary to evaluate the main observable surface characteristics. These are described in detail in the *Manuale dell'Osservatore* (WSL Institute for Snow and Avalanche Research SLF, Davos, 2016) and are summarized in Figure 2-3 using illustrative images (Sauro, 2024):

Figure 2-3 Snowpack's surface characteristics (Source: Sauro, 2024)

2.2 Avalanche Classification

Avalanches are complex natural phenomena, and their classification depends on various factors, including the type of release, the position of the sliding surface, snow moisture, the morphology of the path, and the type of movement (McClung & Schaerer, 2006). Although avalanches can be categorized into distinct types, many intermediate situations do not fit neatly into a single category, making classification a challenging process.

The type of release is one of the main criteria used to classify avalanches and can be divided primarily into:

1. Point release avalanches (loose snow avalanches). These avalanches originate from a single point on the slope, typically involving snow with low cohesion, and form small-scale avalanches. While generally less dangerous in terms of volume, they can still cause significant damage, particularly in the presence of skiers or hikers.

2. Slab avalanches. In this case, the snowpack fractures along a line, often more extensive and elongated. These avalanches are more dangerous because the slabs can break apart during their descent, transforming into powder avalanches. Slab avalanches are typically triggered by external stresses, such as the passage of individuals or vehicles, and occur on slopes with inclinations between 30° and 50° (Rudolf-Miklau et al., 2015).

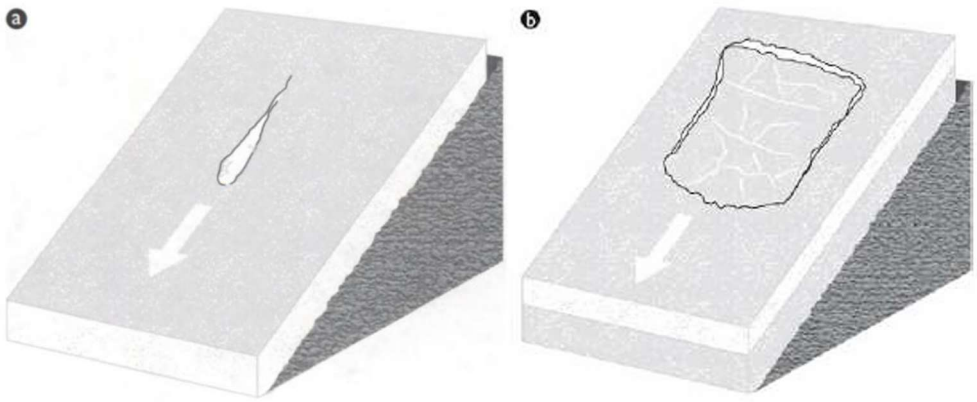

Figure 2-4 Illustration of loose (a) and slab (b) avalanche failure types (McClung and Schaerer, 1953)

Another criterion for classification is the location of the sliding surface within the snowpack:

1. Surface avalanches. The release occurs within the snowpack, with the sliding surface located between different snow layers. This type of avalanche can be dangerous as it may spread over large areas and gain significant velocity (McClung & Schaerer, 2006).

2. Full-depth avalanches. These avalanches originate at the ground surface, potentially involving the entire snowpack. They often occur when the snow is denser or when weaker layers collapse under the pressure of the overlying snowpack (McClung & Schaerer, 2006). Avalanches can also be categorized based on their triggering cause, distinguishing between spontaneous avalanches and those caused artificially or by external factors.

Snow moisture is another crucial factor in avalanche classification. Avalanches can be classified as:

1. Dry snow avalanches. These occur when the snow contains no liquid water and has a low density, usually below 100 kg/m³. Dry snow avalanches are typical during cold periods and can be very fast and destructive.

2. Wet snow avalanches. These occur when the snow contains liquid water, resulting in a significant increase in density (between 300 and 500 kg/m³). Wet snow tends to move more slowly and over shorter distances but exerts greater pressure on obstacles in its path (Giani, 2014). Wet snow avalanches are typical in spring, when temperatures are higher.

The morphology of the avalanche path influences the type of movement and the intensity of the phenomenon (McClung & Schaerer, 2006):

1. Channelled avalanches develop in gullies or couloirs, where the snow flows along a confined path, increasing in velocity.

2. Unchanneled avalanches occur on open slopes without confinement, following the terrain's morphology. They can cover longer distances and involve larger volumes of snow.

The movement of snow during an avalanche can be described in two main forms (Rudolf-Miklau et al., 2015):

1. In case of sliding (or ground-contact), the avalanche primarily slides along the ground, characterized by high density and relatively low velocity. This type of movement typically occurs in loose snow avalanches or wet snow avalanches (Colbeck, 1982).

2. Powder avalanches are characterized by a dense flow of snow and air that moves at very high speeds, up to 100 km/h. Powder avalanches develop in dry snow conditions and can overcome morphological obstacles such as valleys and ridges. Their density is very low (between 1 and 10 kg/m³), but their impact can be devastating due to the velocity and force of the shock wave (Giani, 2014).

In many cases, avalanches do not belong exclusively to a single type but exhibit mixed characteristics. Mixed avalanches combine different types of movements, starting with a sliding component and subsequently evolving into a powder component, or vice versa. This phenomenon is common in the mountainous regions of Italy, particularly during winter periods characterized by heavy snowfall and low temperatures. The transition between these two types of movement makes mixed avalanches particularly difficult to predict and manage (Rudolf-Miklau et al., 2015).

2.3 Avalanche Dynamics Models

The study of avalanche dynamics is a crucial aspect for understanding their behaviour during motion and for developing effective risk mitigation strategies. After identifying the types of avalanches and the causes that trigger them, it is essential to analyse their movement along the path to estimate key parameters such as velocity, runout distance and consequently the size of the accumulation, and impact pressure. This information is indispensable not only for designing protective measures but also for evaluating the forces that an avalanche may exert on infrastructure and populated areas.

To analyse the behaviour of these phenomena, mathematical and numerical models have been developed to simulate avalanche dynamics from initiation to standstill. Since the 1950s, research in this field has given rise to two main modelling approaches: empirical and physical-mathematical. Empirical models rely on statistical analysis of historical events, primarily allowing for the estimation of the runout distance (Barbolini, 2004). However, these models are limited by the need for accurate and representative data for the study area. On the other hand, physical-mathematical models aim to precisely describe avalanche phenomena by considering dynamic variables such as velocity, pressure, flow height, and interactions with terrain and vegetation.

The evolution of physical-mathematical models has led to increasingly sophisticated tools, ranging from analytical to numerical models, capable of simulating avalanche propagation and deposition characteristics in detail. These tools are fundamental for territorial planning and for updating avalanche hazard maps, providing critical support for risk management in mountainous areas (Tanabe et al. 2025).

Empirical models are among the first tools developed for assessing avalanche motion. These approaches do not directly replicate physical phenomena but instead use historical data to extrapolate useful information for predicting future avalanche behavior. Through statistical analysis of documented events, empirical models primarily estimate the maximum runout distance of an avalanche, offering reliable results where detailed and representative historical data are available (Bakkehøi et al., 1983).

In the literature, empirical models are classified into three main categories: regressive, inferential, and comparative (Barbolini, 2004)..

- Regressive models, also known as "Norwegian statistical-topographical models," were introduced by the Norwegian Geotechnical Institute (NGI) and are based on the statistical analysis of observed runout distances in well-documented avalanche sites. These models correlate runout distance with key topographical parameters such as the average slope angle of the starting zone, total vertical drop, and the concavity of the slope profile. An example widely used in practice is the α/β model, which employs the mean slope angle to estimate the maximum distance reached by the snow flow.
- Inferential models apply probabilistic distribution laws, such as Gumbel's law, to avalanche datasets that have been appropriately scaled. These models estimate the probability of an extreme event reaching a specific runout distance by considering the so-called Runout Ratio (RR), a scalar measure linking topographical parameters to flow behaviour.

- Comparative models rely on a comparison method between avalanche sites with similar topographical characteristics. Using the "nearest neighbours" method, the maximum runout distance is estimated as the average of the distances observed in analogous sites. Although less detailed from a statistical perspective, this approach is useful in areas with limited or heterogeneous information.

Physical-mathematical models are fundamental tools for studying and predicting the dynamics of avalanches, from initiation to arrest. These models are primarily divided into point-mass models (centre of mass) and continuum models, each with specific applications and characteristics (Barbolini,2004).

- Point-mass models focus on the motion of the centre of mass of the avalanche along a predefined trajectory, using a single degree of freedom: the curvilinear abscissa of the centre of mass. The dynamics are described by the conservation of momentum law, which can be simplified by assuming a constant mass along the path. Key examples include (Salm et al., 1990; Barbolini,2004):

    - The PCM (Perla-Cheng-McClung) model, which employs the conservation of momentum equation. This approach divides the avalanche path into segments with constant slope, iteratively calculating velocity and runout distance. It is particularly effective for simulations on paths characterized by morphological irregularities.

    - The Voellmy model, which divides the avalanche path into two main phases: the sliding zone, where the avalanche is modelled as an incompressible fluid in steady motion, and the runout zone, where it is treated as a rigid body subjected to deceleration. This model introduces two critical parameters: the Coulomb friction coefficient (μ) and the turbulent friction coefficient (ξ), and it has been widely applied in Switzerland for delineating risk areas.

    - The Voellmy-Salm (VS) (Salm, 1993)model represents an evolution of the previous one, incorporating continuity and momentum equations and dividing the path into three zones: detachment, sliding, and runout. Using adjustable parameters (μ and ξ), it estimates velocity, flow height, and runout distance, proving particularly useful for catastrophic avalanches, although it tends to overestimate in less extreme situations.

- Continuum models, on the other hand, represent the avalanche as a deformable medium in motion and are based on the balance equations of continuum dynamics, such as mass and momentum. This methodology provides a more detailed description of the physical quantities involved, such as velocity, impact pressures, and flow heights. (Barbolini, 2004).

    - Navier-Stokes-based models are a primary category, further divided into Newtonian and Bingham-viscous models, depending on the rheology adopted. These models provide highly precise analyses, though at the cost of significant complexity.

    - Hydraulic or integral models use the Saint-Venant equations to describe the avalanche as a free-surface fluid. These models can also be classified as Coulombian or viscoplastic, depending on the rheological assumptions of the flow.

The choice of the most appropriate physical-mathematical model depends on the type of avalanche being analysed. Dense avalanches are typically described using point-mass or continuum models, while powder avalanches require specific approaches such as single-phase (density current models) or two-phase models (binary mixture models), which allow for the separate analysis of the dynamics of the solid and air components of the phenomenon.

Simpler models, such as point-mass models, are easy to implement and suitable for basic engineering simulations. In contrast, continuum models provide a more realistic and comprehensive description but require a greater amount of data and computational resources.

2.4 RAMMS::AVALANCHE

Figure 2-5 RAMMS Avalanche software, developed by the WSL Institute for Snow and Avalanche Research SLF

The RAMMS (Rapid Mass Movements Simulation) model represents an advanced two-dimensional numerical tool designed to simulate gravitational mass flow phenomena, with application to snow avalanches. Developed by the WSL Institute for Snow and Avalanche Research SLF in Davos, Switzerland, starting in 2005, the model is an evolution of the previous AVAL-1D, providing greater precision in analyses through the adoption of a two-dimensional approach based on three-dimensional digital terrain models (DTM). It is widely utilized for both hazard mapping and practical engineering applications with regard to existing calculation guidelines in Switzerland (Salm et al., 1990)

RAMMS comprises three main modules: RAMMS::AVALANCHE for snow and ice avalanches, RAMMS::DEBRISFLOW for debris and mudflows, and RAMMS::ROCKFALL for rockfall and landslide phenomena. In this study, the RAMMS::AVALANCHE module will be employed, which is specifically developed for simulating mixed avalanches characterized by the presence of two primary layers: the "flowing core" and the "powder cloud." The "flowing core" moves parallel to the slope while laterally expanding; this motion facilitates air entrainment, with heavier particles stabilizing at the lower part, forming the dense core. The "powder cloud," on the other hand, develops subsequently as lighter particles migrate upward with the entrained air, forming a cloud that moves independently of the core. The overall motion of the flow is computed integrally from the release area to the final deposition, accounting for the topography of the avalanche basin (Bühler et al., 2014).

The RAMMS model is based on simplified equations of motion derived from the Voellmy-Salm model (Salm, 1993), which incorporates a Coulomb friction component and a turbulent drag component. To solve these equations, the software employs the finite volume method applied to a grid based on the basin's DTM. The simulations involve certain simplifications: the motion is two-dimensional (without variations along depth), the avalanche mass is considered constant (no erosion phenomena are accounted for), and the velocity profile is rectangular. RAMMS allows high flexibility in defining initial parameters, such as the release area, friction coefficients, cohesion, and snow density. Thanks to its integration with GIS systems, the software facilitates the inclusion of georeferenced spatial data, satellite images, aerial photographs, and topographic maps, enabling detailed modelling of the basin and initial conditions.

The outputs include dynamic variables such as flow velocity, deposit height distribution, impact pressures, and the momentum of the mass. These results can be visualized through two-dimensional and three-dimensional maps, exportable animations, and detailed graphical analyses.

The physical model of RAMMS::AVALANCHE interprets an avalanche as a sliding body on a slope, subject to dissipative forces influenced by a kinematic friction parameter between the mass and the ground (μ) and a viscous-turbulent friction parameter that depends on the square of the velocity (ξ). The frictional force (F) is calculated using the following expression (Salm, 1993; Salm et al., 1990) :

$$F = \frac{\rho g U^2}{\xi} + \mu N$$

Where:

$$N = \rho h g \cos\theta$$

Here, ρ represents the snow density, g the gravitational acceleration, θ the slope angle, h the flow height, and U the flow velocity. The equation also incorporates the centrifugal force generated by terrain curvature, as proposed by Fischer et al. (2012). The centrifugal acceleration (f) depends on the avalanche velocity and terrain curvature and is calculated using the formula:

$$f = U\, K\, U^T$$

The flow velocity of the avalanche, represented by U, is combined with the curvature of the path, described by the matrix K, to determine how the curvature in alla direction affects the flow velocity (through the U^T term). Consequently, the centrifugal force is expressed as:

$$C = \rho\, h\, f$$

This force is added to N in the dissipative force equation F. Generally, C increases friction, slowing down the avalanche on curved slopes and influencing the final deposition location once the channel is exited. The friction parameters (μ and ξ) can be specified by the user or automatically estimated by the software, considering factors such as slope morphology (channel or open slope), elevation, surface roughness, vegetation presence, avalanche volume, and event return period. It is also possible to keep these parameters constant along the entire slope.

The calibration of the parameters in the RAMMS::AVALANCHE model has been performed based on field observations of various avalanches using the SFL (Swiss Federal Laboratories) database and experiments conducted at the Vallée de la Sionne experimental site in the Valais Canton, Switzerland. Within the software, the Voellmy-Salm model has been implemented to include snow cohesion in the avalanche rheology, expressed through the yield stress (τy). To model τy, the parameter N_0 was introduced, enabling the description of ideally plastic materials according to the dissipative force equation:

$$F = \frac{\rho g U^2}{\xi} + \mu N + (1-\mu)N_0 - (1-\mu)N_0 e^{\frac{N}{N_0}}$$

In this equation, μ acts as a "material hardening" parameter. Unlike a formulation based solely on kinematic friction, this expression ensures that F tends to zero as both N and U approach zero. Consequently, an increase in N_0 leads to earlier avalanche stopping, modulated by the value assigned to N_0 (Christen et al., 2017).

3. Avalanche Protection and Risk Mitigation Strategies

3.1 Overview of Avalanche Protection and Risk Mitigation Structures

In recent decades, the urbanization of mountainous areas, particularly in tourist contexts, has contributed to an increased avalanche risk, necessitating the development of appropriate protective systems (Chiambretti, 2018). Historically, populations residing in avalanche-prone areas tended to establish settlements far from avalanche paths (Terzago,2023). However, the expansion of infrastructure has made it necessary to introduce specific measures to safeguard areas affected by these natural events. An "avalanche protection structure" is defined as any defensive intervention located within the avalanche basin (Chiaia & Frigo, 2024), aimed at mitigating the risk to people and exposed structures. Protection solutions are generally divided into three main categories: active structural defences, passive structural defences, and non-structural solutions (Rudolf-Miklau et al., 2015).

Active structural defences intervene directly in the avalanche release zone, with the objective of stabilizing the snowpack and preventing its sliding. The height of these structures must exceed the thickness of the snowpack, incorporating a safety margin. In contrast, passive structural defences do not prevent the avalanche release but aim to reduce its impact on buildings and infrastructure by diverting the snow flow or limiting the stopping distance of the avalanche to prevent structural damage. Stop structures are designed to halt the avalanche by collecting the snow upstream of the barriers.

Non-structural solutions, compared to structural ones, are generally less expensive. For example, seasonal road closures, particularly in alpine passes or roads connecting villages inhabited only during the summer, eliminate the risk to individuals without requiring significant investments. Other non-structural measures include the installation of sensors to detect avalanche movements in specific gullies, which activate traffic-blocking signals. Additionally, artificial avalanche triggering, conducted to prevent large-scale events, represents another non-structural measure. This operation, which requires careful evaluation of snowpack conditions and the evacuation of people at risk, can be carried out using explosives, gas cannons, or sound waves. In Italy, the use of explosives is strictly regulated, prompting a preference for alternative techniques. These may be either fixed or mobile (helicopter-transportable or drone-operated), powered by gas or utilizing pyrotechnic explosives. Some examples include fixed cable systems (Catex®), fixed gas systems (GazEx®), and DaisyBell®. (Chiaia & Frigo, 2024).

Although not classified as a protection structure, the protective forest is worth mentioning, as it helps prevent avalanches in forested areas by stabilizing the snowpack and reducing the avalanche's energy, thereby limiting its length (Chiaia & Frigo, 2024). However, it is important to note that forests cannot halt medium- or large-scale avalanches already in motion, nor can they entirely prevent snow release within forested areas.

Another classification of protection measures is based on their temporal effectiveness, distinguishing between permanent and temporary structures. Permanent structures provide constant protection, regardless of the season or the intensity of the avalanche risk. These structures may function by hindering avalanche release or propagation, or by decelerating, diverting, or

retaining the snow flow. Temporary structures, on the other hand, are limited in duration and designed for specific, provisional situations to minimize the consequences of an avalanche event.

When deciding on the most appropriate protection solution, it is essential to consider the target to be protected and its actual exposure risk to avalanches. Equally significant is the evaluation of costs associated with monitoring and maintaining the structure, as well as its integration into the surrounding environment, respecting the pre-existing ecology and landscape.

A further classification of protection measures considers the location of the structures within the different zones of the avalanche path: the start zone, the track, and the runout zone. In the release zone, protective measures include structures for stabilizing and supporting the snowpack, such as snow bridges, racks, nets, and umbrellas, which reduce the risk of release by preventing snow movement.

Figure 3-1 Snow retention structures in Nassfeld, Austria (Photo: Mattia Matzutzi)

Additional interventions include measures to control snow transport caused by wind, such as deflectors and snow fences, which modify wind activity on the snowpack, altering snow deposition and limiting the formation of hazardous accumulations.

Figure 3-2 Wooden avalanche windbreak (Photo: iStock.com / futurewalk)

In the flow and deposition zones, protection measures include deflecting structures, stopping structures, and specialized defence structures. Deflecting structures, such as dams or guiding walls, aim to direct the avalanche flow toward a safe area, protecting infrastructure or reducing the energy of the snow flow to facilitate its stopping over shorter distances. Their effectiveness is higher for the dense flow component of the avalanche but limited for the powder component.

Figure 3-3 Guiding walls (Source: Provincia Autonoma di Bolzano)

Stopping structures, on the other hand, are built perpendicular to the avalanche flow direction and function by collecting the avalanche material within a reservoir formed upstream, preventing its downstream expansion.

Figure 3-4 Stopping structure (Source: Provincia Autonoma di Bolzano)

Braking structures, such as containment walls, mounds, wedges, braking teeth, and check dams, aim to reduce the flow velocity, dissipating energy and decreasing the destructive power of the avalanche.

Finally, there are specialized defence structures, such as avalanche tunnels, which will be discussed in detail later.

Figure 3-5 Avalanche tunnel, Slovenia (Photo: Miha Pavšek, ZRC SAZU)

3.2 Analysis of Avalanche Impact Forces on Infrastructure

Avalanches generate significant pressures during their interaction with obstacles, constituting one of the primary causes of damage to inhabited areas and infrastructure. The analysis of the impact with an obstacle reveals that avalanches develop dynamic pressure, which, for calculation simplicity, is often approximated as stationary and thus time independent.

A critical aspect involves solid materials transported by the flow, such as rocks, ice blocks, or trees, which can cause significantly higher-pressure peaks upon impact compared to those generated by the rest of the flow. Equations proposed by Rudolf-Miklau, Sauermoser and Mears (2015) are used to calculate the pressure exerted by an avalanche on an obstacle, distinguishing between wide and narrow obstacles and classifying avalanche motion based on type (McClung & Schaerer, 2006) (dense, powder, or mixed).

The impact force of an avalanche on a structure is generally correlated with the kinetic energy of the flow, which depends on the flow's velocity and density, which may be either local or averaged. In this context, reference pressure is introduced, defined as the static pressure exerted by the avalanche flow on a vertical surface of 1 m². Impact or collision pressure is proportional to this reference pressure, with coefficients varying based on several parameters: the obstacle's position relative to the flow direction (e.g., frontal, lateral, or vertical impact), the obstacle's shape and size, the flow's nature (dense or powder), and the flow regime (inertial, gravitational, or intermediate) (Rudolf-Miklau et al., 2015).

Analogous to fluid dynamics, impact pressure is calculated as follows:

$$p = \frac{1}{2} C \rho v^2$$

where ρv^2 represents the dynamic pressure, the product of the avalanche flow density ρ and the square of its velocity v^2, while C is the aerodynamic drag coefficient, dependent on snow type and the obstacle's shape and dimensions.

When a structure is struck by solids carried by the avalanche mass, the localized impact load must be considered. This load is modelled as an equivalent static force applied over a footprint with a 25 cm diameter, its intensity related to the avalanche's reference pressure:

- 100 kN for a reference pressure of 30 kPa (3 t/m²)
- 66 kN for a reference pressure of 20 kPa (2 t/m²)
- 33 kN for a reference pressure of 10 kPa (1 t/m²)

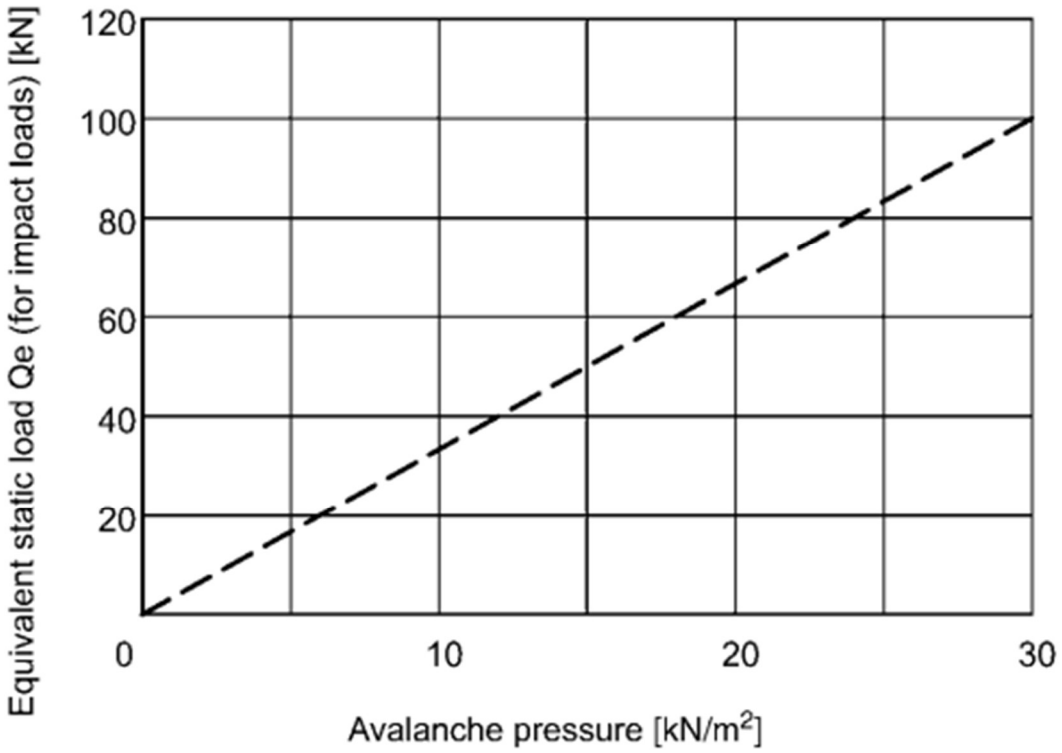

Figure 3-6 Avalanche pressure over equivalent statistic load (Rudolf-Miklau et al,.2015)

This force acts in conjunction with pressures induced by the avalanche flow.
For dense avalanches impacting wide obstacles, much of the flow is stopped by the obstacle, exerting dynamic pressure on the exposed area, while a smaller portion bypasses the obstacle. The dynamic pressure on wide obstacles orthogonal to the flow direction is given by:

$$p_f = \rho v^2$$

However, in the initial moments, the avalanche exerts a peak pressure p_{peak}. According to Rudolf-Miklau et al. (2015), this peak pressure should be considered as a supplement to the stationary pressure, as it can occur during the first milliseconds of impact on an obstacle. It is suggested that this short-duration peak pressure can be up to three times the mean pressurecalculable as:

$$p_{peak} = 3\, p_f$$

When the obstacle is not orthogonal to the flow direction, the normal and tangential pressure components must also be considered. These depend on the angle (α) between the flow direction and the exposed face of the obstacle and on the obstacle's friction coefficient:

$$p_n = \rho_f v_f^2 \cdot \sin^2 \alpha$$

$$p_t = \mu \cdot p_n$$

The friction coefficient (μ) varies by material: 0.30 for snow-on-snow or snow-on-ground

surfaces, and 0.40 for rough surfaces. Dense avalanches may partially climb the obstacle due to dynamic impact, rising to a height referred to as the "climbing height":

$$h_{dyn} = \frac{v_f^2}{2g\lambda}$$

where λ represents the momentum loss factor, accounting for friction between the avalanche and the obstacle during the ascent. It is 1.5 for dry snow avalanches and ranges from 2 to 3 for wet snow avalanches.

For narrow obstacles, most of the avalanche flow bypasses the obstacle. Examples of narrow obstacles include trees, high-voltage poles, or telephone poles. The dynamic pressure of avalanche flow on a narrow obstacle is calculated as:

$$p_f = c_d \frac{\rho_f \cdot v_f^2}{2}$$

where c_d is the aerodynamic drag coefficient, which depends on the obstacle's shape. The force exerted by the avalanche on the obstacle is obtained by multiplying pressure by the impacted area A:

$$p_f = A\, c_d \frac{\rho_f \cdot v_f^2}{2}$$

Even with narrow obstacles, dense avalanches may climb partially along the obstacle to the following height:

$$h_{dyn} = \frac{v_f^2}{2g\lambda} f_{b/df}$$

where b and df are the obstacle width normal to the flow direction and the avalanche flow height, respectively, and $f_{b/df}$ is a reduction factor dependent on these parameters.

Table 3-1 Reduction factor f (Rudolf-Miklau et al., 2015)

b/d_f	0.1	0.5	1.0	2.0	≥3
f	0.1	0.4	0.7	0.9	1

In evaluating pressures exerted by powder avalanches, it is essential to note that the saltation and suspension layers have significantly lower densities than dense avalanches, though they move at higher velocities. The saltation layer has a density between 20–50 kg/m³, while the suspension layer varies from 3–15 kg/m³. Powder avalanches are mixtures of ice particles, air, and snow grains; in this context, solid particles may directly impact the obstacle surface rather than following the airflow. Pressure is calculated similarly to dense avalanches, with an additional dynamic pressure coefficient dependent on flow velocity, particle size, and concentration, ranging

between 0.5 and 1. In cases of uncertainty, it is conventionally set to 1.

The height of the powder snow layer is directly proportional to the avalanche path length (l_{path}) and the square of the avalanche velocity (v), and can be expressed as:

$$h_p = 10^{-4} l_{path} v^2$$

As highlighted in the Table 3-2 the height of the powder snow layer is also influenced by the slope gradient, with thicker layers associated with steeper inclines.

Table 3-2 Dependence of the powder snow layer on the slope gradient (Rudolf-Miklau et al., 2015)

Slope inclination	*dh/dx*
10°	0.05
30°	0.10
50°	0.15

The distribution of pressures along the longitudinal and transverse directions of the flow varies due to topographical factors and turbulence. The latter can generate pressure spikes that reach values up to twice the mean pressure.
When the avalanche flow surpasses or bypasses an obstacle, four primary effects must be considered:

- Overriding the obstacle: The avalanche exerts a hydrostatic overpressure, which depends on the mass rather than the velocity, with values typically ranging between 0.5 and 2 kPa.
- Effective pressure: This depends on the shape and orientation of the obstacle relative to the flow direction. In general, the pressure decreases from the centre of the exposed surface toward the edges.
- Negative dynamic pressure on lateral walls and the top of the obstacle: This can be expressed as:
- $p_{suc} = -\frac{1}{2}\rho_p v_p^2$
- Shear stress: When the structure remains within the sliding zone and the saltation layer is pronounced, the shear stress on the obstacle must be considered. This can reach values of approximately 0.5–5 kPa.

Avalanches often do not occur as purely dense-flow or purely powder avalanches. Instead, they frequently manifest as mixed events, combining dense snow layers, saltation layers, and airborne layers. To analyse the forces exerted by each component of a mixed avalanche, a distinct separation between the layers is assumed, allowing for individual calculations of the actions exerted on an obstacle, as previously outlined for dense-flow and powder avalanches, illustrated in Figure 3-7.

Finally, while the direct action of the snowpack on an obstacle is generally negligible compared to the avalanche itself, it is important to consider that the forces exerted by the avalanche can be transmitted to the surrounding snowpack. This generates a pressure p_H, which, as shown in the figure, is distributed linearly to a depth equal to twice the height of the dense-flow layer.

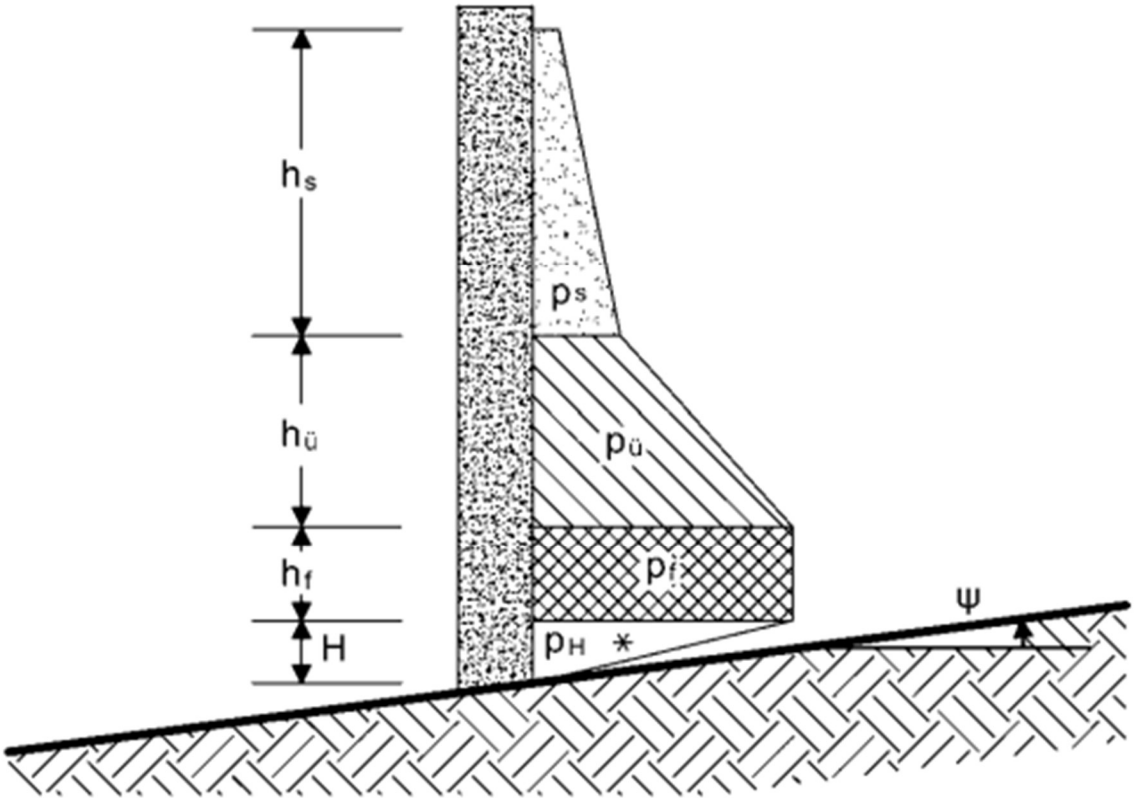

Figure 3-7 Diagram of the pressures exerted on an obstacle by the various layers forming a mixed avalanche (Rudolf-Miklau et al., 2015)

3.3Effects of Avalanches on Protective Tunnels

Avalanche galleries and tunnels are essential infrastructures for protecting communication routes located in avalanche tracks o runout zones. Their primary function is to allow the avalanche flow to pass over the structure, preserving the infrastructure below from damage. These structures are particularly effective in areas with a large avalanche release zone and a well-defined interference zone, characterized by limited longitudinal development in the runout and deposition areas (Chiaia & Frigo, 2024).

Figure 3-8 Podljubelj avalanche tunnel, Slovenia (Photo: Mattia Matzutzi)

To ensure smooth flow of the avalanche, it is crucial that galleries or tunnels maintain a minimal elevation profile. In many cases, the roofs of these structures are designed to align with the natural slope, facilitating smooth passage of snow. Unlike completely enclosed tunnels, avalanche galleries often feature openings along their structure, which distinguish their function and appearance. Additionally, these structures are frequently integrated with diversion systems that reduce the length of the gallery itself. The combined effect of the diversion works helps precisely delineate the avalanche runout area, protecting the gallery portals as well (Chiaia & Frigo, 2024).

The design of such structures is based on established guidelines, such as the Swiss "Guidelines for Avalanche Actions on Protection Galleries" (ASTRA, 2007), issued by the Federal Roads Office (OFROU).

The Figure 3-9 illustrates a schematic representation of the geometric features and fundamental parameters for the design of an avalanche gallery. Key parameters include:

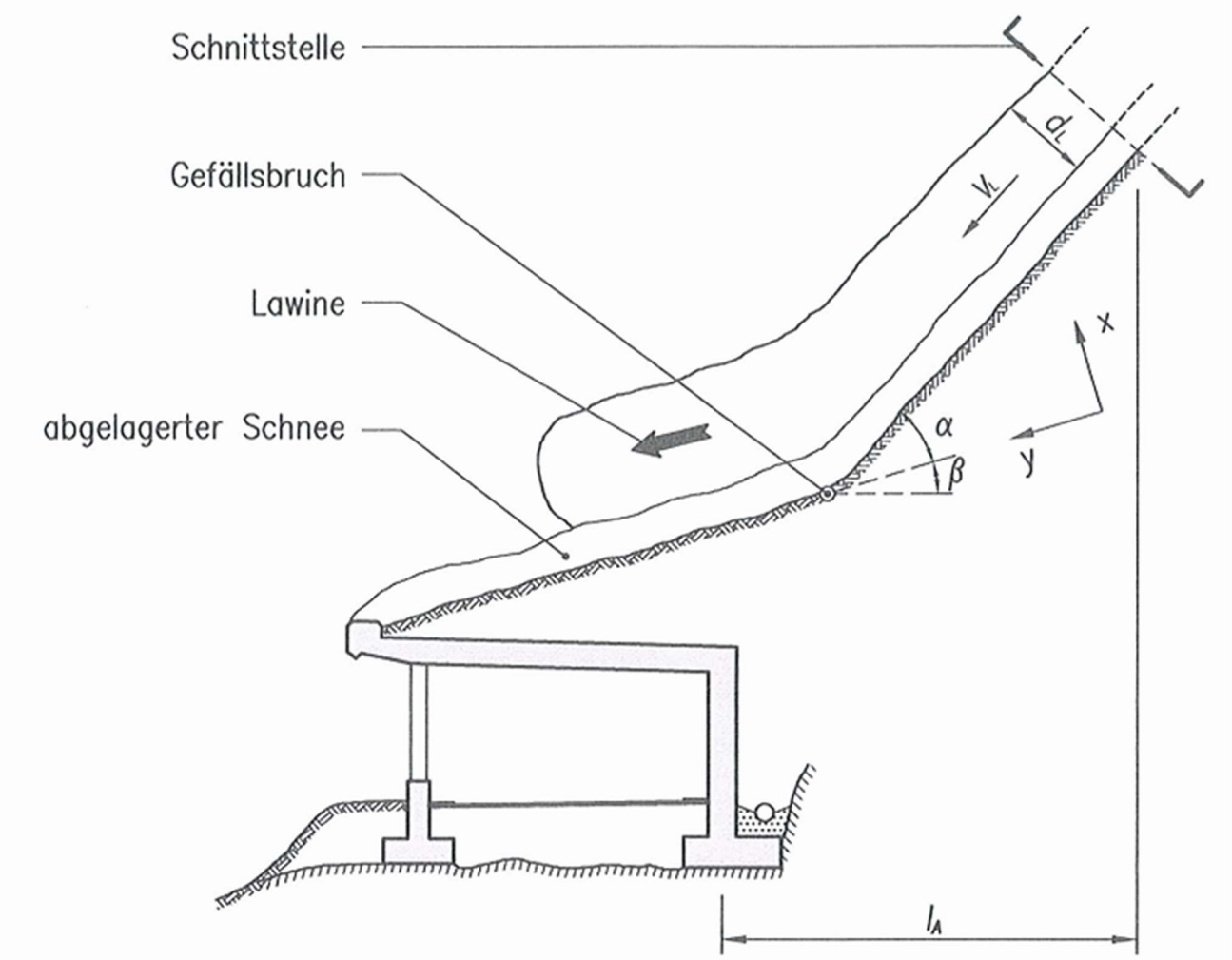

Figure 3-9 Fundamental parameters for the design of an avalanche gallery (Source: ASTRA,2007)

- I_A : horizontal distance between the critical section of the structure (referred to as "Schnittstelle") and the gallery, representing the point of interaction between the avalanche and the structure.
- d_L: height of the avalanche flow, corresponding to the thickness of the moving snowpack.
- V_L: velocity of the avalanche at the moment of impact.
- α: avalanche deviation angle induced by the structure.
- β: slope inclination in the gallery area.

The diagram also highlights the slope break point (*Gefällsbruch*) and the avalanche flow (*Lawine*) interacting with the structure. It is also important to consider the snow that accumulates above or near the gallery (*Abgelagerter Schnee*), which may influence structural loads.

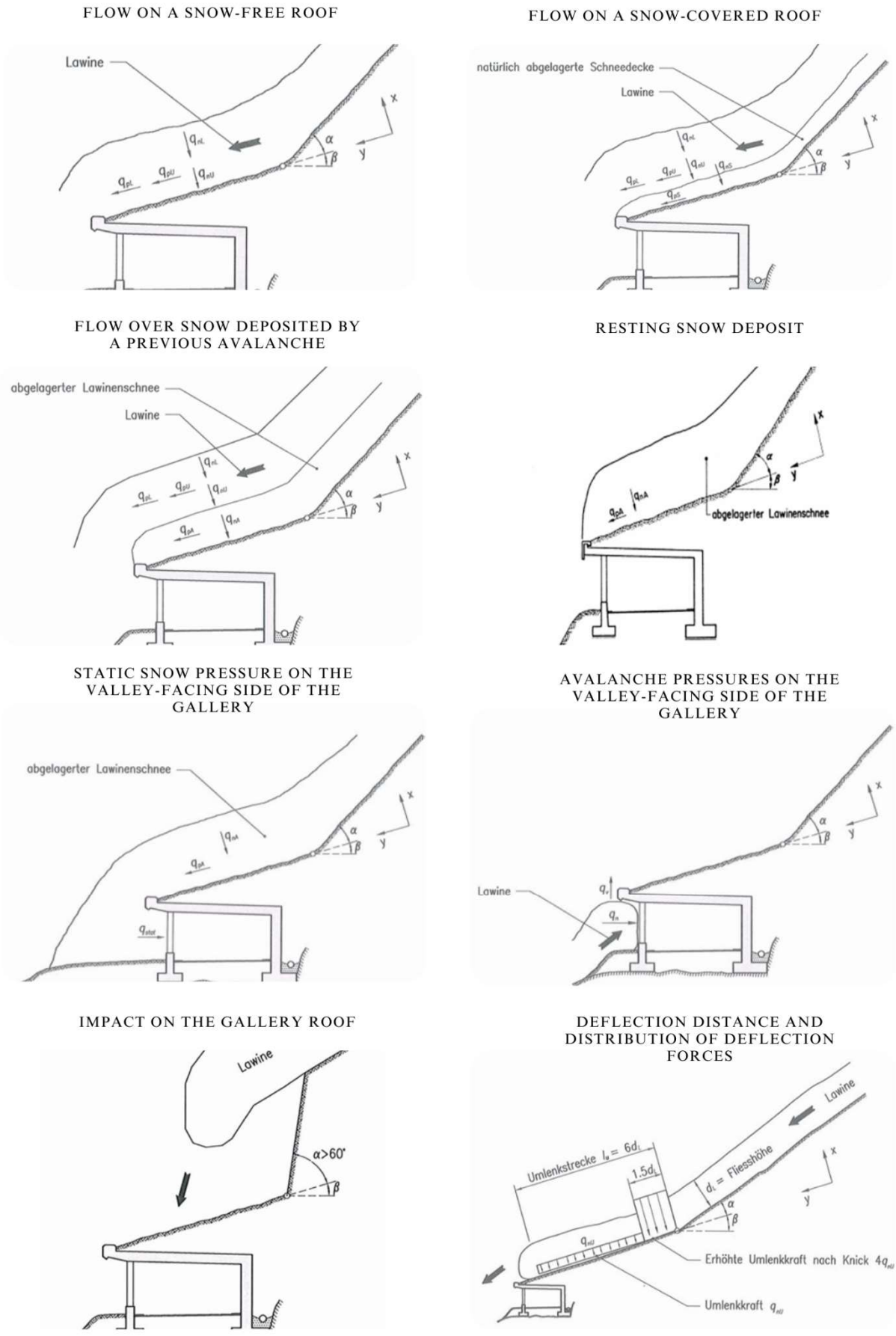

Figure 3-10 Different snow/avalanche interactions with tunnels and the forces (Source: ASTRA, 2007)

To calculate the pressures exerted by snow on galleries, it is essential to define the average volumetric loads (γ) of snow based on its physical characteristics. Reference values are:

Table 3-3 Average volumetric loads (γ) of snow based on its physical characteristics

Snow Type	Density (γ) $\frac{kN}{m^3}$
Moving avalanche (dry snow)	3
Moving avalanche (wet snow)	4,5
Natural accumulated snow	4
Deposited avalanche snow	5

Additionally, friction coefficients (μ) must be considered for different sliding surfaces. These values depend on the type of snow and the surface material:

Table 3-4 Friction coefficients (μ) for different sliding surfaces

Surface Type	Friction Coefficient (μ)
Snow on dry snowpack	0,2
Snow on wet snowpack	0,35
Snow on smooth surface (dry) (e.g., concrete, grass)	0,25
Snow on smooth surface (wet) (e.g., concrete, grass)	0,45
Snow on rough surface (dry) (e.g., rocky blocks)	0,35
Snow on rough surface (wet) (e.g., rocky blocks)	0,55

Based on these parameters, the pressures acting on the tunnel under different conditions are calculated as follows:

Natural accumulated snow:

- Perpendicular pressure:

$$q_{nS} = \gamma d_s \cos\beta$$

- Parallel pressure:

$$q_{pS} = q_{nS} \tan\beta$$

Deposited avalanche snow:

- Perpendicular pressure:

$$q_{nA} = \gamma d_A \cos\beta$$

- Parallel pressure:

$$q_{pA} = q_{nA} \tan\beta$$

Moving avalanche:

- Perpendicular pressure:

$$q_{nL} = \gamma\, d_L \cos\beta$$

- Parallel pressure:

$$q_{pL} = \mu\, q_{nL}$$

Avalanche deflection force:

- Perpendicular pressure:

$$q_{nU} = \frac{\gamma\, d_L\, v_L^2 \sin\alpha}{6\, d_L\, g}$$

- Parallel pressure:

$$q_{pU} = \mu\, q_{nU}$$

4. Thesis Objective

This study aims to analyse the functionality of the tunnel located in the Podljubelj area, with particular attention to the risks associated with snow accumulation resulting from avalanche events. In the past, significant avalanches have led to the deposition of large amounts of snow along the roadway near the tunnel entrance and exit, causing severe traffic disruptions and compromising transit between Slovenia and Austria. In addition to obstructing circulation, these phenomena pose a concrete threat to road users' safety, as individuals caught near the tunnel during a major avalanche event could be engulfed by the snow mass.

Figure 4-1 Podljubelj Tunnel from the drone (Source: Blaž Komac, ZRC SAZU)

To this end, this research utilizes simulations conducted with RAMMS software to determine the snow and meteorological conditions that favour snow deposition on the road network. Initially, an estimate was made, with a certain degree of approximation, of the probability of a road user being impacted by the snow mass based on vehicle size and avalanche magnitude. This enabled a risk assessment associated with vehicular transit. Subsequently, a comparative analysis was conducted between the costs of constructing a new avalanche protection structure, characterized by minimal or no maintenance costs, and the budget currently allocated by the Slovenian government for deploying snow removal equipment following avalanche events. The analysis also considered the economic losses due to road closures and the actual risk to human safety.

5. The Case Study of the Podljubelj Avalanche Tunnel, Slovenia

5.1 The Study Area

5.1.1 Geographical, Historical, and Economic Characteristics of the Podljubelj Valley

The Podljubelj Valley, located in the Gorenjska region in the far north of Slovenia, extends along a north-south axis, forming a natural corridor nestled between the towering peaks of the Karawanks. It spans approximately 15 kilometres in length and covers a total area of about 50 km², primarily within the municipality of Tržič. The valley is bordered to the west by the Karawanks mountain range and to the east by foothills separating it from the Sava River valley.

The region north of Tržič is defined by the Košuta ridge (Košutnikov turn, 2133 m) and the Begunjščica ridge (Veliki vrh, 2060 m). Predominantly composed of Triassic limestones and dolomites, the area exhibits distinct karst hydrography. The slopes are steep, ranging from 33° to 55°. The tree line is at 1700 m above sea level, where *Pinus mugo* and alpine meadows begin. The northern slopes of Košuta and Begunjščica form steep rock walls with scree deposits at their base. The area is utilized for mountain pastures, tourism, and recreational activities (Natek et al. 2010).

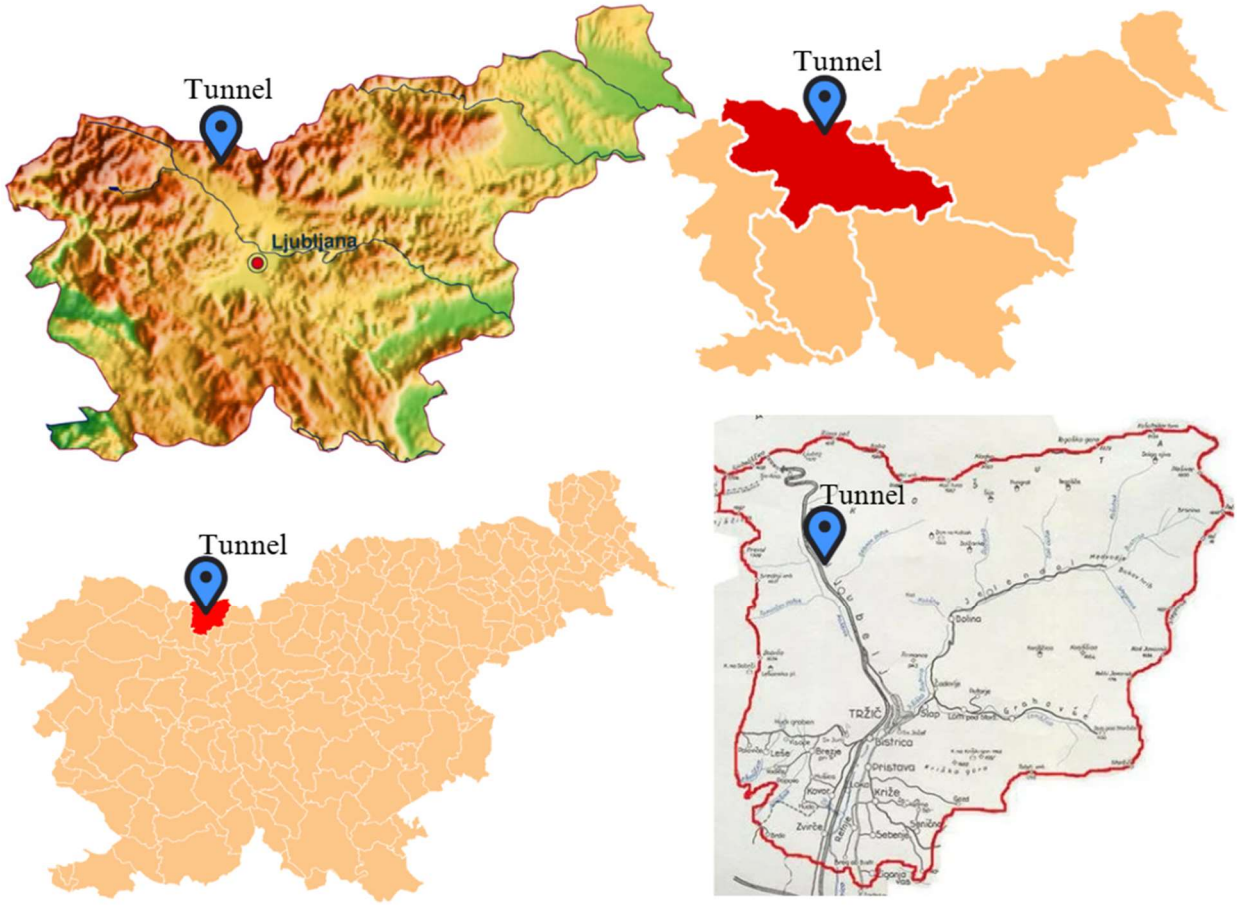

Figure 5-1 Geographical Location of the Podljubelj Tunnel. Top Left: Physical map of Slovenia. Top Right: Gorenjska region in Slovenia. Bottom Left: Municipality of Tržič, Slovenia. Bottom Right: Focus on the Municipality of Tržič

In terms of elevation, the area ranges from approximately 700 meters above sea level near Tržič to its highest point at Ljubelj Pass, situated at 1,369 meters. This mountain pass has played a strategic role as a communication route between Slovenia and Austria since Roman times, facilitating trade and the transport of goods.

During World War II, the area gained military significance, being extensively utilized by German forces, who established a concentration camp there. The Ljubelj concentration camp stands as a tragic testament to the Nazi repressive machine in occupied territories. Established in 1943 as a subcamp of Mauthausen, this detention and forced labour site was used for the construction of the Ljubelj tunnel. Today, the labour camp site serves as a memorial, featuring a museum that preserves tools, documents, and original structures such as barrack foundations.

The two commemorative obelisks located at 1,370 meters at Ljubelj Pass were erected to celebrate the construction of the tunnel commissioned by Emperor Charles VI of Habsburg in the 18th century, replacing an earlier gallery dating back to 1560.

Figure 5-2 Memorial obelisks erected to celebrate the construction of the Ljubelj tunnel (Source: Wikipedia)

5.1.2 Geomorphological Aspects and Natural Hazards

From a geomorphological perspective, the Podljubelj Valley exhibits a typical fluvial morphology, sculpted by mass movements and the erosive action of waters. The region is currently subject to active morphogenetic processes such as landslides, debris flows, and fluvial erosion by the Tržiška Bistrica torrent. The processes are related to high precipitation. In Javorniški Rovt daily maximum precipitation for a 10-year return period is 148 mm and 188 mm for a 50-year period. Therefore, specific discharge exceeds 50 l/s/km^2 in the Sava basin, and reaches maximum at 2000 l/s/km^2. This implies high variability of water discharge and fast increase of water discharge in local streams. Consequently, high erosion areas (3/4 and 4/4 categories) comprise 78 % of the area of Tržič Municipality.

Figure 5-3 Embankment and net fences against rockfall about 300 metres north of the Podljubelj tunnel (Photo: Miha Pavšek, ZRC SAZU)

The surrounding mountains, including Mount Begunjščica (2,060 meters), are characterized by Triassic and Jurassic limestone formations. In the area, rocks comprise of limestone, dolomites, breccia, marls, shales and diabase, ceratophyre and porphyries and tufs, and clastic rocks, such as sandstones, claystone, breccia and conglomerates of different geological age. Quaternary sediments are represented by moraine material and younger fluvial sands and slope sediments (Geological map of Slovenia, https://ogk100.geo-zs.si/).

Snow-related phenomena, including avalanche formation and detachment, are particularly significant. In the lowland part of the Tržič area there are an average of 40 to 60 days with snow cover per year, in the hilly part between 60 and 100 (Podljubelj 78 days, Jelendol 81 days), and between 100 and 150 days in the mountains. The first snow is common in October, and the last in May. On average there are about 12–15 days with more than 10 cm of new snow, in general snow cover is

lower than 25 cm (96,7% of time with snow cover). In 1971–2009 period there were 412 events with 25–50 cm snow cover (2,9%) and 61 events with 50–75 cm snow cover, usually in the period from January to February. In the mountains, snow conditions are influenced by the wind, snowdrifts and snow under the walls persist for long time. The number of days with snow cover depends on air temperature and precipitation. With altitude, the temperature drops on average, while precipitation increases. Total height of newly fallen snow is between 140 to 280 cm in the hilly part, and from 280 to over 420 cm in the mountains. Data on the maximum height of the snow cover with a return period of 50 years are similar. Extreme snow cover in the Tržiška Bistrica valley can reach a height of 100 to 150 cm, while it can be higher than 400 cm in the mountains. In the period 1971–2009 the longest duration of snow cover in Podljubelj was 130 days. On average, there were 92 days with snow cover in Jelendol from 1971–1980, 85 in the decade 1981–1990, and 70 days in the decade 1991–2000 (Natek et al. 2010).

Table 5-5: Variability of the annual number of days with snow cover in the season in the period 1971–2009 in cm (Natek et al. 2010, p. 23)

	Average	Standard deviation	Minimum	Maximum
Tržič	67	27	11 (1988/89)	110 (1985/86)
Podljubelj	78	30	14 (1988/89)	130 (1979/80)
Jelendol	81	33	15 (1988/89)	138 (1979/80)

The area records annual precipitation exceeding 2,000 mm in water equivalent, with substantial snow accumulation on particularly steep slopes, favoring frequent avalanche events. Some of them were recorded by the media. An avalanche hit the road leading through Ljubelj and the last house below Ljubelj Pass was swept away on March 8th, 1909. On January 12th, 1978, an avalanche covered the road to Ljubelj. On January 15th, 1885, a giant avalanche buried 20 people with horses and carts. In the region, the deadliest avalanche occurred on March 29th, 1937, on the Storžič Mountain which claimed nine lives. Avalanches are common on the northern slopes of Begunjščica. On January 11th, 1977, an avalanche buried a group of 28 students and three teachers, five students and a teacher died (Malešič 2005; Komac et al. 2023).

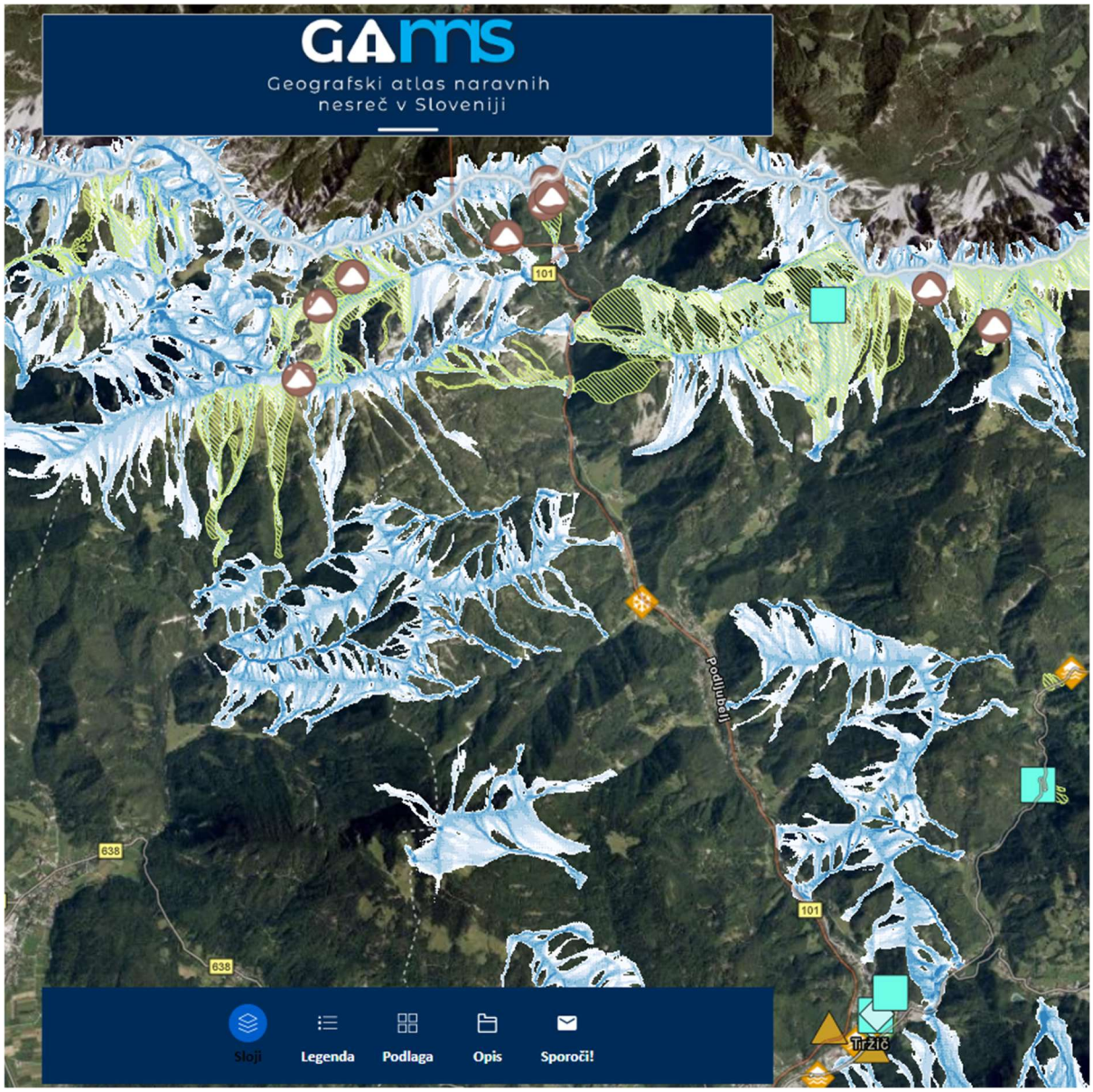

Figure 5-4 Avalanche hazard and selected avalanche events in the Podljubelj Valley north of Tržič (Source: Komac et al. 2023)

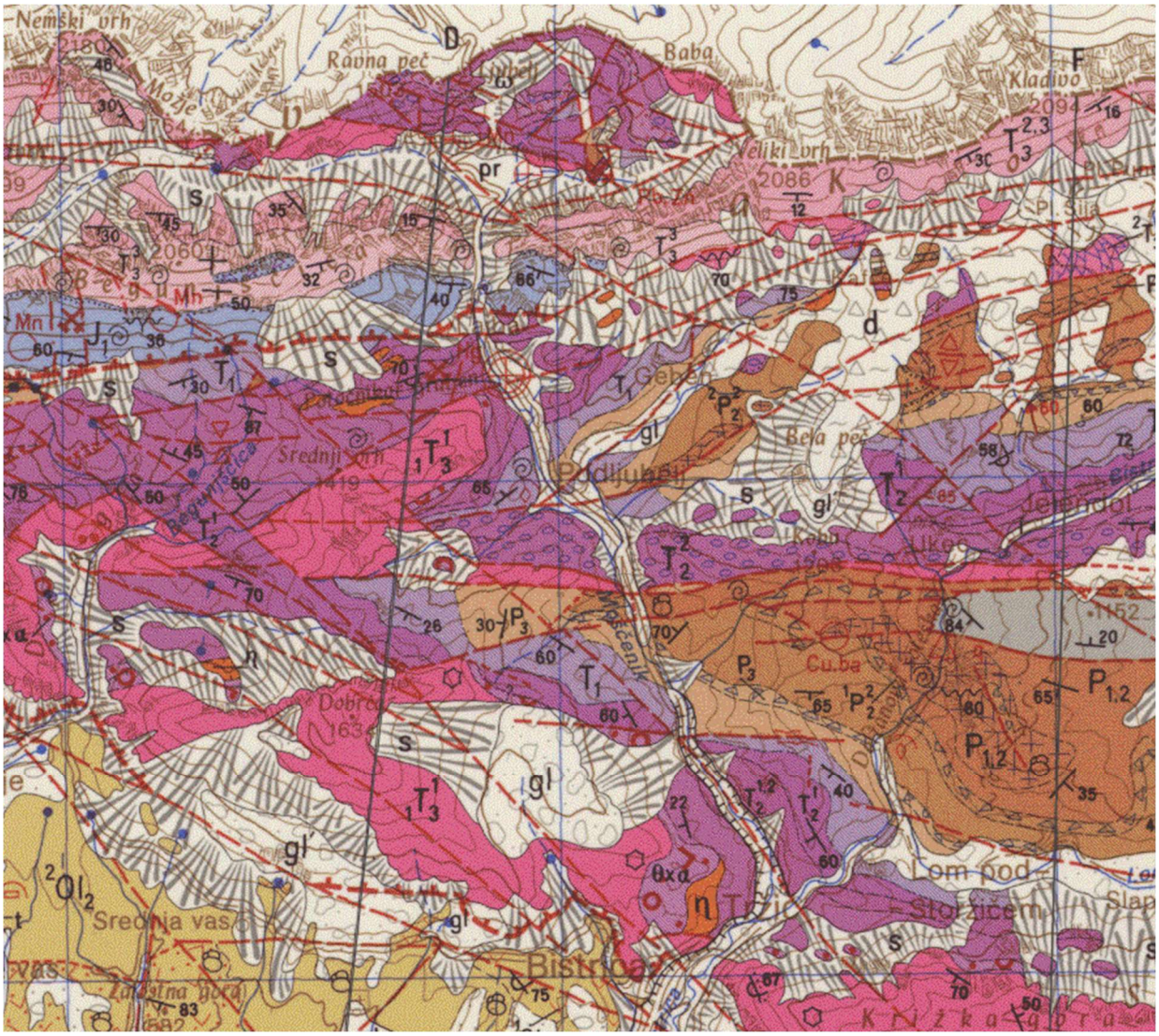

Figure 5-5 Geology of the Podljubelj Valley between Tržič and the Sava Valley in the south and Slovenia–Austria border in the north (Source: Geološka karta Slovenije, https://ogk100.geo-zs.si/)

5.1.3 Contemporary Economic Activities

The present-day economy of the Podljubelj Valley primarily relies on tourism and the utilization of forest resources. During both summer and winter seasons, the area attracts a large number of visitors due to its hiking trails, cycling routes, and proximity to renowned ski resorts. In recent years, tourism infrastructure has seen significant development, with the construction of alpine lodges, hotels, and agritourism facilities.

Ljubelj Pass, currently closed to vehicular traffic, is accessible only on foot or by bicycle. The route to the pass follows a gravel path of approximately 2.5 km, featuring 13 switchbacks, leading to a wooden shelter that offers a panoramic view of the Ljubljana and Klagenfurt basins.

Figure 5-6 Ljubelj wooden shelter (Photo: Visit Tržič)

5.1.4 The First Project Proposals

After the Second World War, the increase in road traffic and the high risk of avalanches along the stretch of road under consideration made the need for suitable protective infrastructure evident. In this context, an artificial avalanche tunnel was built in in the valley below the Ljubelj Pass 1962 to protect one of the most exposed segments of the road.

Initial design solutions for mitigating avalanche risk were varied. One of the initial proposals involved installing snow barriers in the detachment zones, as indicated by the continuous red lines in Figure 6-7, to reduce the volume of potentially mobilizable snow. An alternative considered was the adoption of controlled release systems in trigger areas, capable of generating small, controlled avalanches to limit snow accumulation and the risk of larger spontaneous events.

For the flow zone, the installation of deflecting wedges (red triangles in Figure 5-7) was evaluated, designed to reduce avalanche velocity and impact forces by fragmenting the snow mass and mitigating its interference with underlying roadways. However, logistical challenges due to steep slopes and difficult access to both the detachment and flow zones complicated the implementation of such measures. Consequently, the decision was made to construct an avalanche tunnel, despite its higher design and construction costs compared to other proposed solutions. This choice proved to be more practical and, provided that the tunnel's dimensions were adequate, ensured significantly more effective protection against avalanche risk.

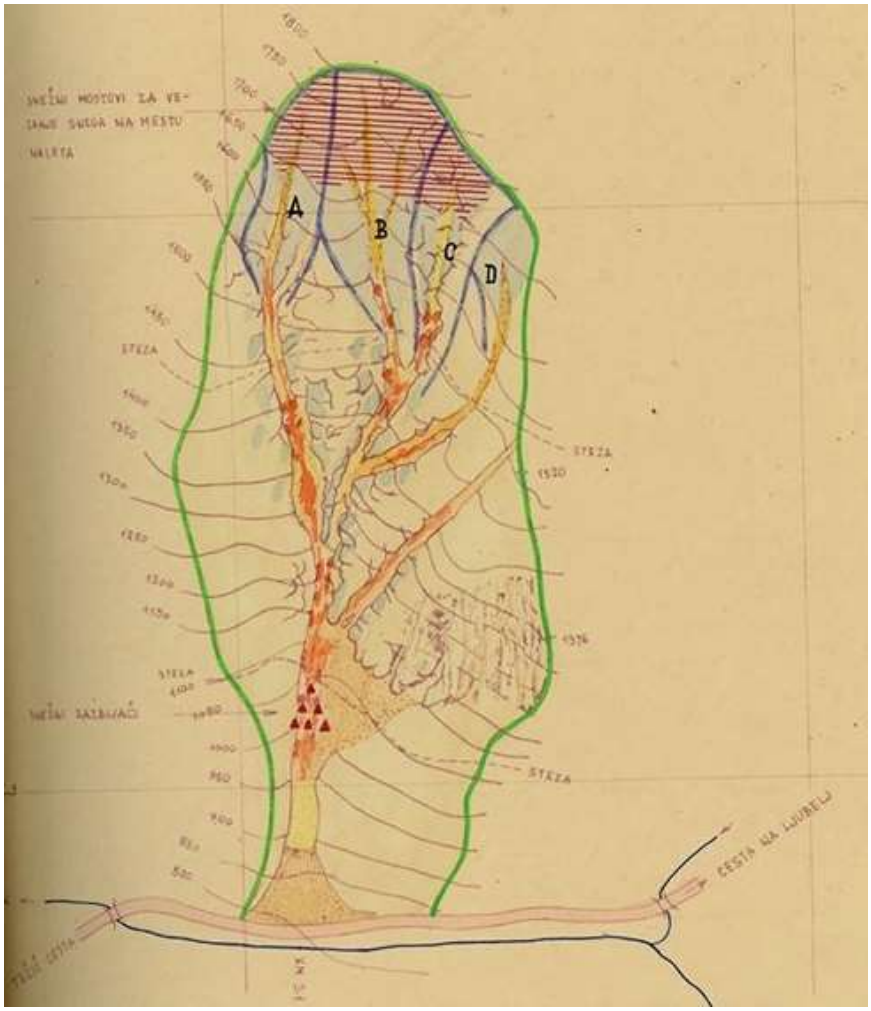

Figure 5-7 First proposals for defence works (Source: SNEŽNI PLAZOVI. I. DEL dipl. ing. Jože Pintar, Podjetje za urejanje hudournikov Ljubljiana, 1968)

5.1.5 Structural Features of the Avalanche Tunnel

The tunnel, built in 1962, extends for a length of 130 meters and was designed, according to the initial project draft, to withstand avalanches with a maximum snow volume of 150,000 m³. The structure is made of reinforced concrete and features a lowered arch section, a configuration that allows for even load distribution and high resistance to stresses from snow accumulation and potential landslides. The roadway inside the tunnel is approximately 7.5 meters wide, while the tunnel opening reaches 12 meters. The intrados height varies between 4.5 and 5 meters, allowing passage for heavy vehicles such as trucks and buses.

Figure 5-8 Podljubelj Tunnel. View from below: from Slovenia to Austria (Source: SNEŽNI PLAZOVI. I. DEL dipl. ing. Jože Pintar, Podjetje za urejanje hudournikov Ljubljiana, 1968)

On the orographic left side, a concrete parapet delineates the roadway, while the right side of the structure is directly anchored to the mountain slope. The latter has been shaped with an inclination that facilitates snow runoff, thus preventing critical accumulations on the road surface.

Figure 5-9 Podljubelj Tunnel. Top view: from Austria to Slovenia (Source: SNEŽNI PLAZOVI. I. DEL dipl. ing. Jože Pintar, Podjetje za urejanje hudournikov Ljubljiana, 1968)

5.1.6 Functional Limitations of the Gallery and Cases of Avalanche Interference

Since the early years following its construction, it became evident that the length of the gallery was insufficient to effectively protect the road in the event of exceptionally large avalanches. Photographic documents dating back to 1965 show instances where snow accumulations obstructed the gallery entrance, temporarily compromising its functionality.

Figure 5-10 Removal of snow obstructing the tunnel entrance. Estimated period 1965 (Source: SNEŽNI PLAZOVI I. DEL dipl. inq. Jože Pintar, Podjetje za urejanje hudournikov Ljubljiana, 1968)

Further evidence of these critical issues is reported in the publication *Pogubna razigranost 1984–1994*, which includes a photograph of the 1984 event, accompanied by the description: "The snow avalanche demonstrates that the gallery built under Ljubelj is too short and was therefore covered with snow."

Figure 5-11 Photo from the book Pogubna razigranost 1984–1994, snow wall at the tunnel entrance (Photo: Aleš Horvat)

Moreover, the avalanche event registry concerning damages to road infrastructure cites significant episodes, including one in February 1972 and a series of incidents recorded between 1975 and 1985. In particular, one case is mentioned where a bus was trapped inside the tunnel due to snow accumulation, further highlighting the structural limitations of the infrastructure in relation to high-magnitude events.

Table 5-6 Extract from the avalanche accident register

1984	26-feb	Begunjski plaz (predor)	cesta	zasutje zaradi prekratkega predora	višina cca. 7 m, podobno tudi 9/2 1986, višina le 2 m, takrat je zasulo avto; med 1975-85 enkrat v predoru zaradi tega obtičal tudi avtobus
1984	*26-feb*	*Begunj avalanche (tunnel)*	*Route*	*overflow due to a tunnel that is too short*	*height approx. 7 m, similar also on 9/2 1986, height only 2 m, at that time a car got stuck; in 1975-85 a bus got stuck in the tunnel once as a result*

In the absence of an official avalanche cadastre, the use of historical data has proven to be an essential element in determining a possible return period for the avalanche under study. The analysis conducted has shown that the avalanche in question exhibits a potential annual recurrence; however, over the

past sixty years, from the construction of the tunnel to the present day, only two documented events have been confirmed to have interfered with road traffic. Since the primary objective of this study is to assess the impact of avalanches on the road network, a return period of 30 years was adopted for subsequent simulations and analyses, as it was deemed more representative for RAMMS simulations and the subsequent risk assessment.

5.1.7 Geomorphological Analysis of the Avalanche Basin

The analysis of the avalanche under study has allowed for the identification of eight detachment zones, the sliding path, and the accumulation area.

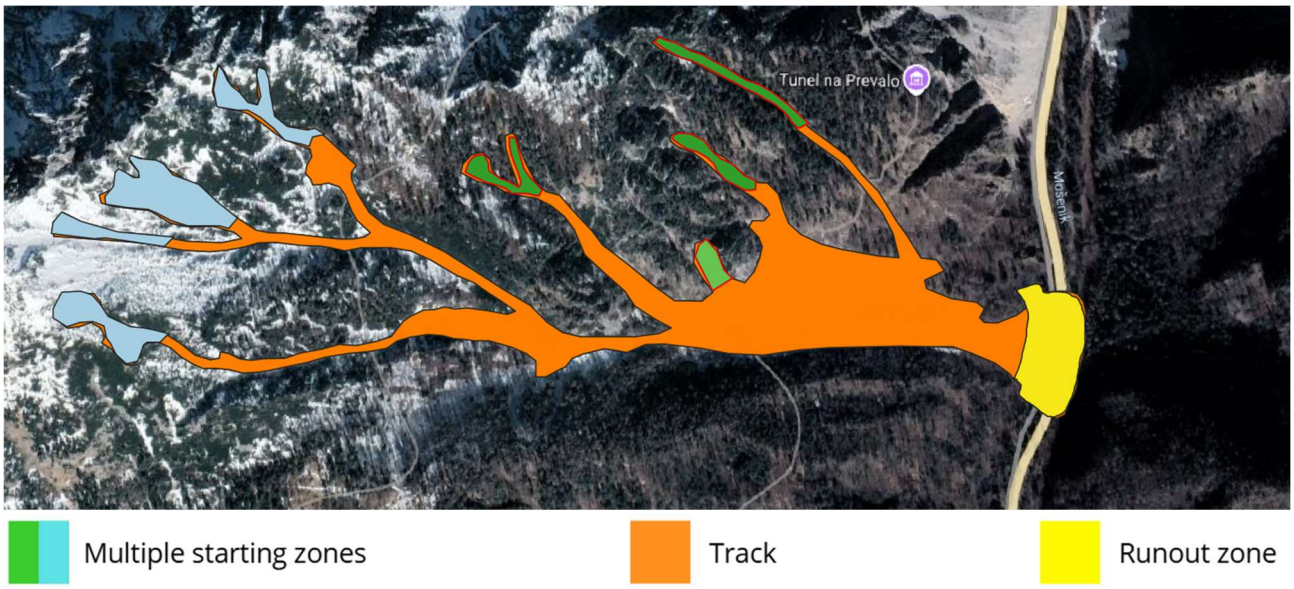

Figure 5-12 Avalanche basin

The most important characteristics of the avalanche are reported in the Table 5-7.

Table 5-7 Avalanche description (Source: ZRC SAZU)

Column (Slovenian)	Translation (English)	Description	Value
id	ID	Unique identifier of the avalanche	1681
tip	Type	Type of avalanche (e.g., normal, slab, wet, etc.)	Normal
povrs_m2	Surface area (m²)	Total area affected by the avalanche in square meters	141477,54
vis_povp	Average altitude (m)	Average altitude of the avalanche area	1236,41
vis_min	Minimum altitude (m)	Lowest altitude of the avalanche area	806,17
vis_max	Maximum altitude (m)	Highest altitude of the avalanche area	1776,55
nak_povp	Average slope (°)	Average slope of the affected area	36,73
nak_min	Minimum slope (°)	Lowest slope in the affected area	8,41
nak_max	Maximum slope (°)	Highest slope in the affected area	58,84
veg_povp	Average vegetation cover (%)	Average percentage of vegetation in the avalanche area	3,06
veg_min	Minimum vegetation cover (%)	Minimum percentage of vegetation cover	0,05
veg_max	Maximum vegetation cover (%)	Maximum percentage of vegetation cover	33,37

raba_ime	Land use name	Description of the type of land use	Dry open land with special vegetation cover
raba_m2	Land use area (m²)	Total area covered by this land type	71566,38
raba_%	Land use percentage (%)	Percentage of total area corresponding to this land type	50,58
kam_ime	Rock type name	Predominant rock type	Paleozoic and Mesozoic massive limestone
kam_m2	Rock type area (m²)	Area covered by this rock type	62630,51
kam_%	Rock type percentage (%)	Percentage of total area covered by this rock type	44,27
lse_ime	Stratigraphic unit name	Name of the geological formation	Ridge limestone with corals
lse_star	Geological age	Geological period	Upper Triassic (Rhaetian)
lse_m2	Stratigraphic unit area (m²)	Area covered by this geological formation	62630,51
lse_%	Stratigraphic unit percentage (%)	Percentage of total area covered by the formation	44,27
do_stavb	Distance to buildings (m)	Average distance to the nearest buildings	444,62
do_ceste	Distance to roads (m)	Average distance to the nearest roads	21,64
do_gozdc	Distance to forests (m)	Average distance to the nearest forests	729,71
do_planp	Distance to pastures (m)	Average distance to the nearest pastures	559,19

On the opposite slope, on the left bank, there is another avalanche basin which, although it has never directly interfered with traffic, has a deposit area coinciding with that of the main avalanche.

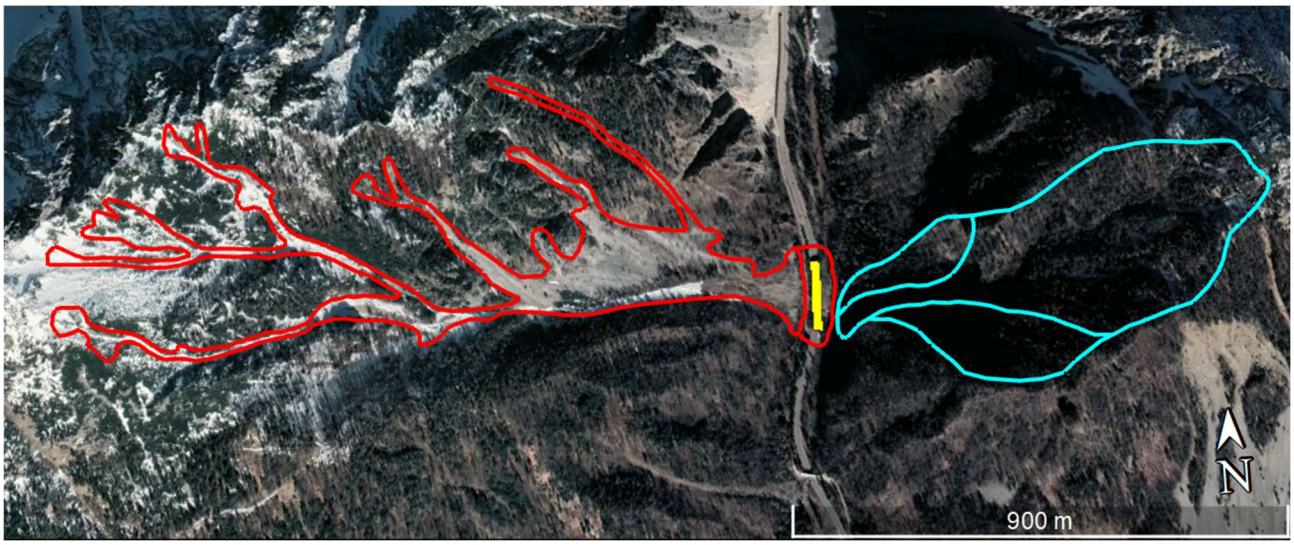

Figure 5-13 The avalanche basin on the opposite slope is shown in blue, and the tunnel in yellow

Currently (01-2025), the site shows the presence of a debris deposit composed of gravel, rocks, and

logs, potentially capable of influencing the bypass that the tunnel is intended to create. The tunnel is overgrown by trees. The analysis of the avalanche path present in GANNS suggests a more limited deposit area compared to reality. However, a careful evaluation of the digital terrain model highlights how even the avalanche on the left bank interacts with the tunnel, depositing a significant amount of material that could significantly influence the dynamics and extent of the avalanche event.

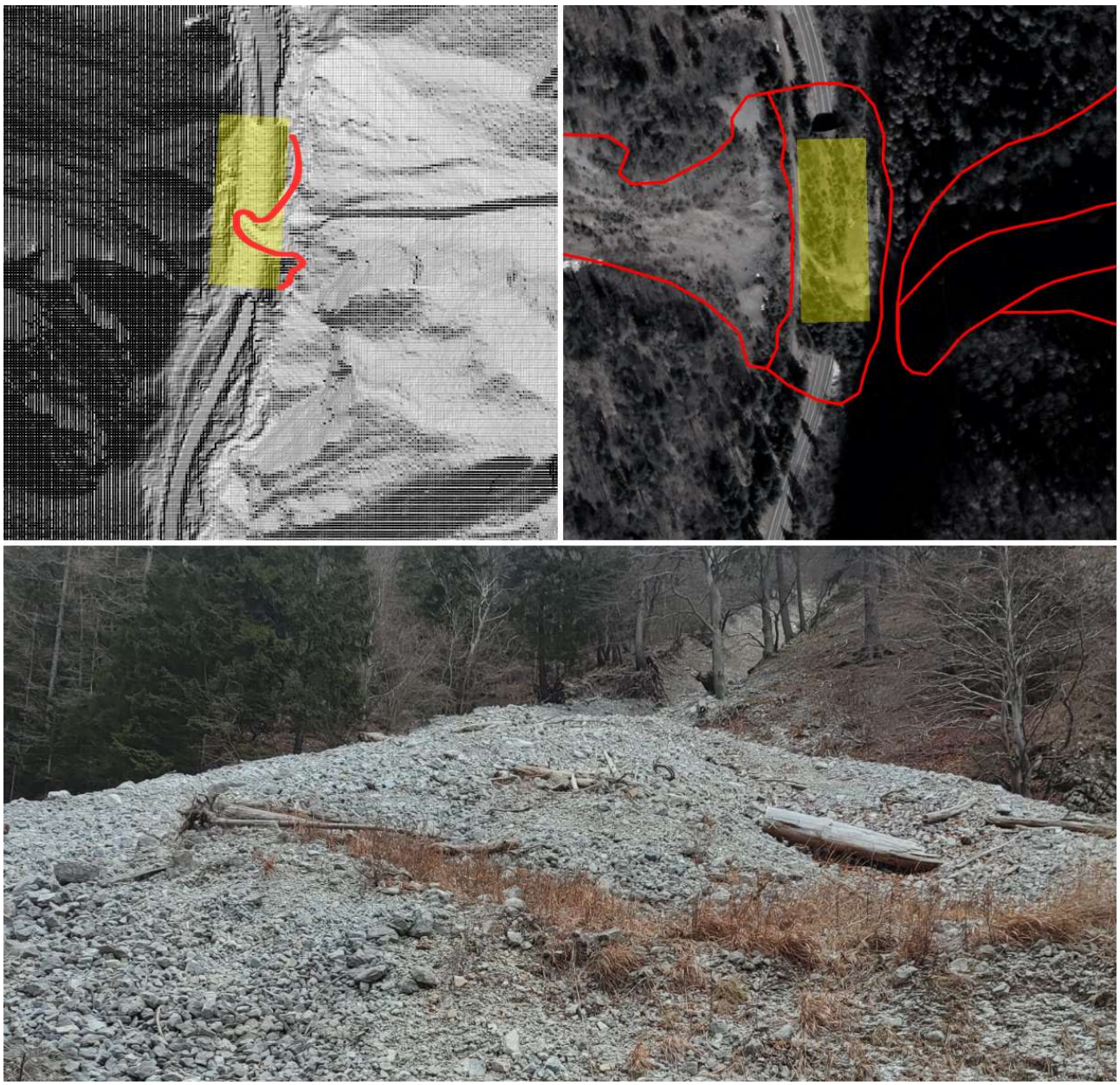

Figure 5-14 Overlay of the Avalanche Deposit Zones. Top Left: Deposit highlighted on the DTM. Top Right: Avalanche basins present on the GANNS. Bottom: Photo of the deposit taken from above the tunnel (Photo: Mattia Matzutzi)

5.1.8 Geomorphology of the Release Areas

The study area presents a complex morphology, characterized by eight potential avalanche initiation zones distributed between 1,200 and 1,780 meters above sea level. All detachment, sliding, and deposit zones are located on the right bank, with a southeastern exposure. The release areas were identified based on the avalanche path recorded in the GANNS database and analyzed considering morphological parameters such as inclination, curvature, and slope. This procedure was manually conducted by applying the Potential Release Areas (PRA) method proposed by Maggioni et al. (2002).

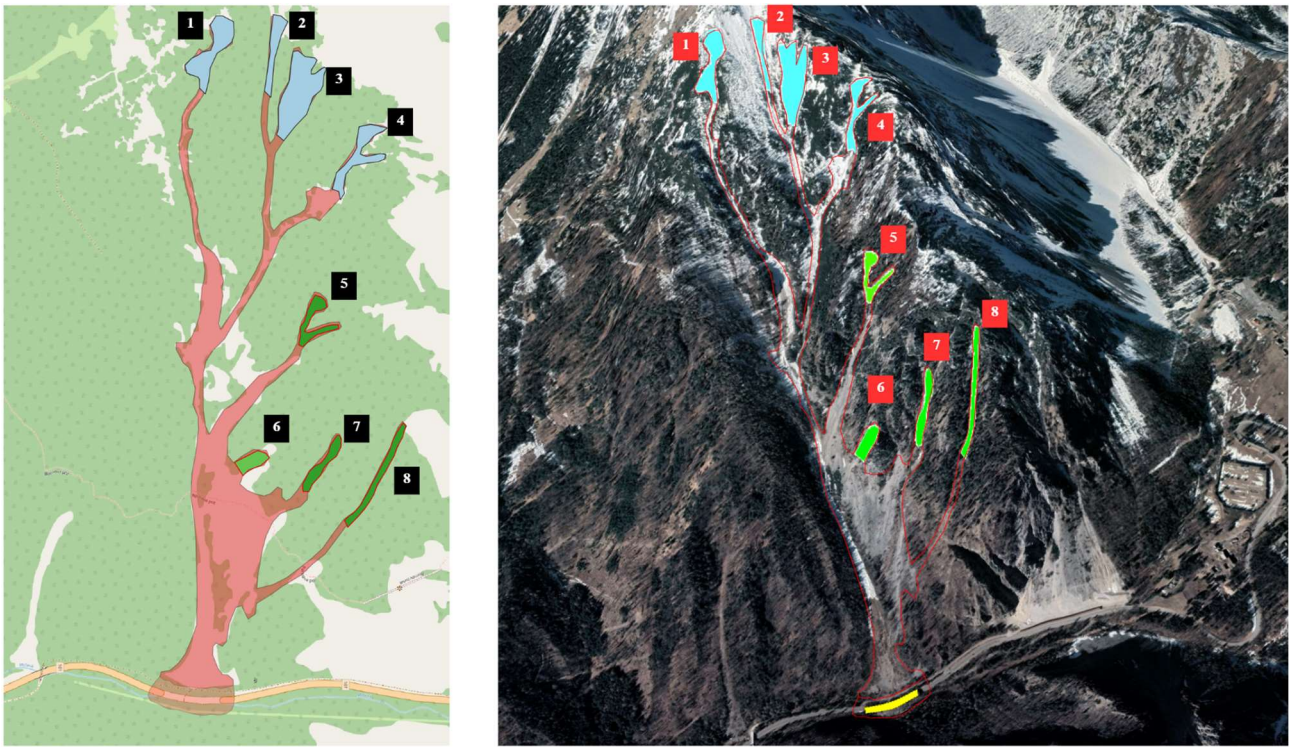

Figure 5-15 Potential relase areas

The average inclination of the initiation zones varies significantly, ranging between 39% and 55%. Zones 1, 2, 3, and 4 feature rocky exposure with almost no vegetation.

Figure 5-16 Potential release areas. Slope angle and altitude of 1, 2, 3 and 4

Table 5-8 Characteristics of potential release areas 1,2,3 and 4

Release area	Area (m²)	Mean slope angle (°)	Mean altitude (m)
1	8024,6	41,51	1724,02
2	3790,3	39,15	1728,42
3	13215,8	40,59	1678,00
4	7269,6	48,99	1634,79

Zones 5, 6, 7, and 8 are characterized by denser and more mature vegetation cover.

Figure 5-17 Potential relase areas. Slope angle and altitude of 5, 6, 7 and 8

Table 5-9 Characteristics of potential release areas 5,6,7 and 8

Release area	Area (m²)	Mean slope angle (°)	Mean altitude (m)
5	5719,9	55,23	1397,80
6	3781,4	55,17	1173,3
7	3838,7	47,76	1198,43
8	5028,4	44,07	1252,35

Table 5-10 Comparison table between Figure 5-7 and Figure 5-15

Release areas in the 1962 design	Release areas in this work	Assessment
A	1	The A corresponds to the 1
B	2 and 3	In this work, B has been divided into two potential detachment areas 2 and 3.
C	4	The C corresponds to the 4
D	5	The D corresponds to the 5, the 1962 drawing also denotes the absence of mitigation works for this branch.

5.2 Analysis of Meteorological Conditions and Snow Data

For the study of snow-meteorological conditions, historical data from the Podljubelj meteorological station (680 m above sea level) were used, covering the period from 1975 to 2019. Since there are no specific data on temperature, wind, and humidity for the study area, data from the Lesce station (515 m), located about 8 km away in a straight line, were used. Although climatic conditions may vary significantly between adjacent valleys, a comparison of snowfall series showed a strong correlation, making the use of these data acceptable for the present study.

During the analysed period, twelve significant snowfalls were identified, characterized by a snow accumulation of more than 60 cm and a fresh snow deposit of at least 20 cm in one of the five days within the considered time window.

Table 5-11 Twelve significant snowfall events between 1975 and 2019, each with a snow depth of at least 60 cm and 20 cm of new snowfall within a five-day period.

Year	Start Date	End Date
1976	February 11	February 16
1984	February 22	February 27
1984	February 28	March 4
1985	January 11	January 16
1986	February 27	March 4
1987	January 11	January 16
1987	February 16	February 21
1987	March 16	March 21
1999	February 6	February 11
2005	December 24	December 29
2013	February 20	February 25
2014	January 29	February 3

For each of these snowfalls, trends in temperature, snow depth, humidity, and wind speed were examined, following the methodological criteria proposed by Volk Bahun (2020). It is essential to highlight that avalanche phenomena can be triggered by a multitude of concurrent factors and that, consequently, there is no single formula capable of guaranteeing the certainty of a snow detachment.

The analysis of avalanche events therefore requires a methodological approach that considers the dynamic interaction of meteorological and snow-related variables over time. As an illustrative example, the specific case of February 1976 is reported:

- Temperature: The observed thermal trend reveals a progressive decrease in temperatures between the fifth and third day preceding the hypothetical event, followed by a gradual rise up to the moment when, theoretically, the avalanche could have been triggered. This thermal behaviour suggests a possible contribution of temperature variation to the destabilization of the snowpack, particularly through snow metamorphism phenomena that could alter the cohesion between layers and, consequently, favour a possible detachment.

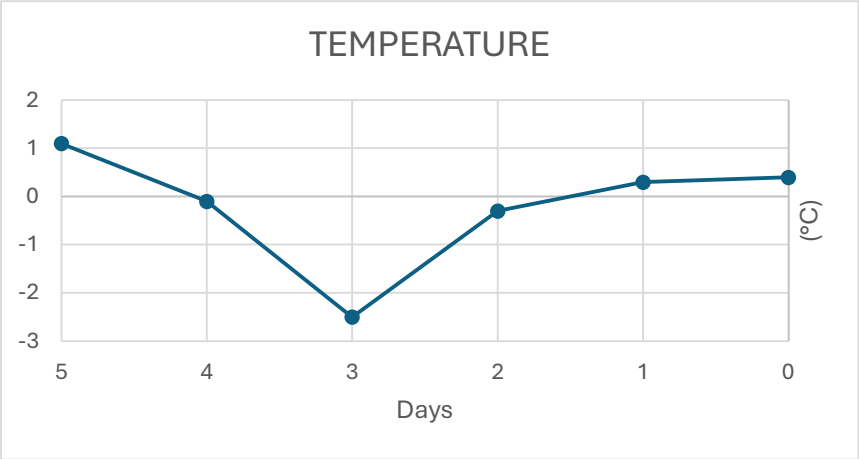

Figure 5-18 Temperature variation between February 11 and February 16, 1976

- Snow Depth: The evolution of the snow cover in the days preceding the events shows a progressive increase in the total snowpack height, with a particularly significant accumulation of new snow in the hours immediately before the detachment. This observation suggests that abundant snowfall can play a crucial role in overloading the snow mass, increasing the risk of structural instability of the deposit and making an avalanche trigger more likely.

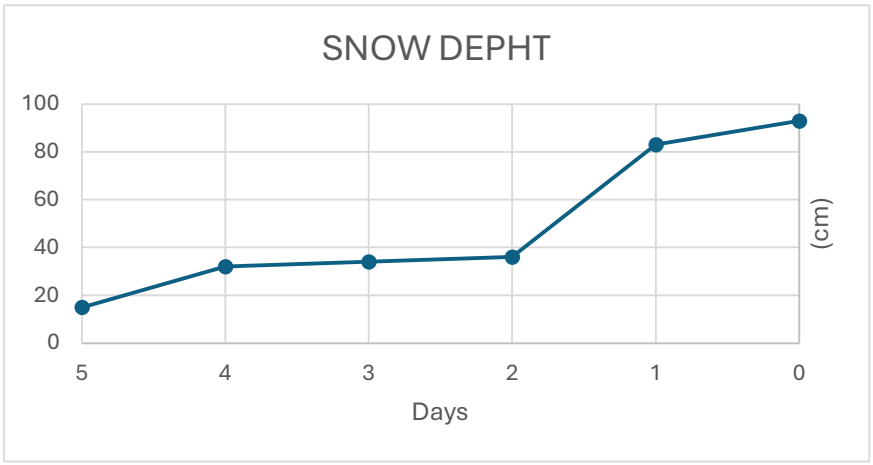

Figure 5-19 Snow depth variation between February 11 and February 16, 1976

- Wind: The wind conditions recorded near the event are characterized by marked variability. Although wind is a key factor in redistributing fresh snow and forming accumulations and cornices, it does not necessarily represent a unique and determining element for triggering an avalanche. However, data analysis shows a general trend of increasing wind intensity in the days immediately preceding the hypothetical event.

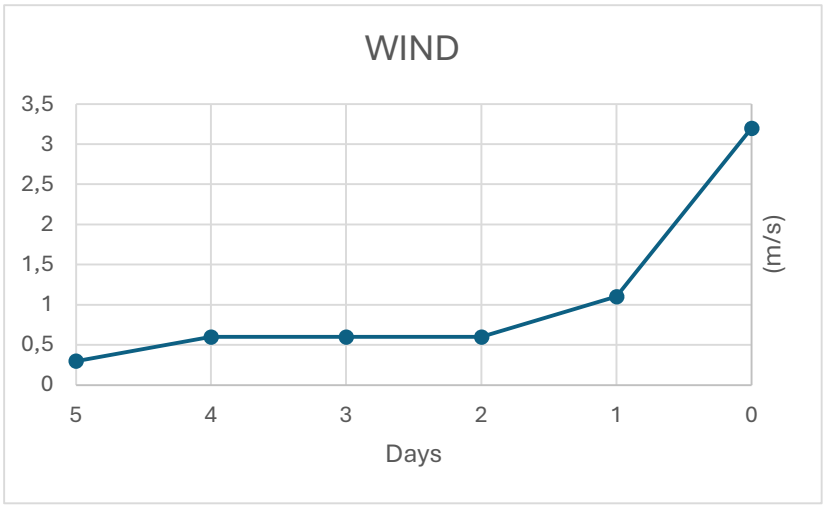

Figure 5-20 Wind variation between February 11 and February 16, 1976

- Humidity: Humidity variation is a crucial parameter in evaluating the stability of the snow deposit. An increase in humidity could significantly influence cohesion between layers, making the snow heavier and promoting the formation of mechanically weak zones. In particular, the infiltration of liquid water resulting from melting processes or wet precipitation could increase the risk of detachment, reducing the shear strength of the snow and making an avalanche event more likely.

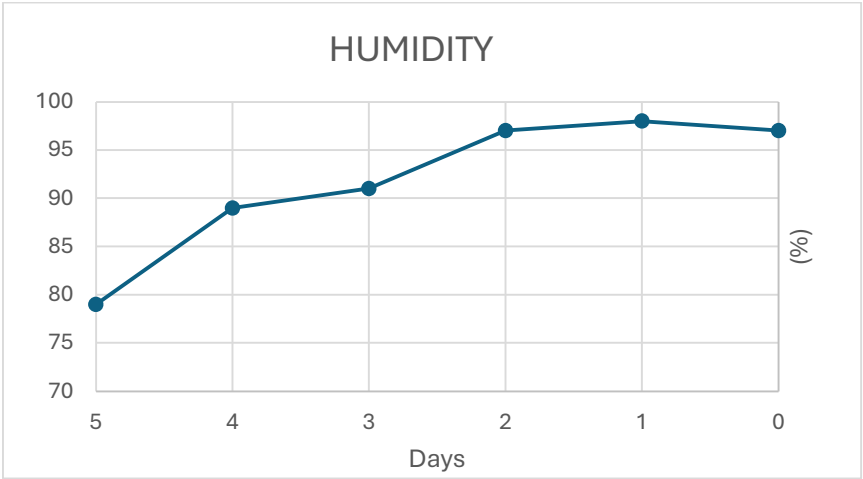

Figure 5-21 Humidity variation between February 11 and February 16, 1976

The analysis of the different considered time windows allowed for the identification of five intervals that meet the previously outlined criteria, making them compatible with the occurrence of potential avalanche events. These periods are reported in the following table:

Table 5-12 Potential avalanche events

Year	Start Date	End Date	Snow depth (cm)
1976	February 11	February 16	93
1984	February 22	February 27	97
1987	January 11	January 16	96
1999	February 6	February 11	101
2013	February 20	February 25	72

To estimate the amount of snow accumulated in the detachment area, which is significantly higher in altitude than the meteorological station, a precipitation increase coefficient was determined as a function of altitude.

The adopted methodological approach involved analysing cumulative precipitation at the meteorological stations of Tržič (480 m) and Podljubelj (680 m) and calculating the variation coefficient of precipitation with altitude k, with direct proportionality based on the 200-meter altimetric variation of the two used stations. This process was applied to eight-year intervals, covering the period from 1976 to 2020. The results obtained indicate that, on average, the increase in precipitation is about 10% for every 100 meters of elevation gain over the eight years. Although this value is subject to a high degree of approximation, it was considered significantly high.

Consequently, the same calculation was repeated over a shorter period, corresponding to a 30-day time window for each of the previously identified avalanche events. The analysis was conducted considering the 15 days before and the 15 days after the start and end date of each event in Table 6-12 , to which the 5 precipitation days characterizing the snow episode were added. In the case of the most significant snowfalls, the obtained precipitation increase coefficient with altitude was 0.03, corresponding to an increase of 3% for every 100 meters of elevation gain. This parameter proved useful in attempting to estimate the snow depth in the detachment areas.

The calculation of snow depth was performed using the following formula:

$$S(z) = P\ (1 + k\ \Delta z)\ R$$

Where:

- P represents the precipitation in mm at the reference altitude, derived from meteorological station data;
- k is the estimated increment coefficient, equal to 3%;
- Δz indicates the altitude difference expressed in hundreds of meters, which in this case is approximately 9 (since the sum of the base altitude of 680 m and the 900 m elevation gain results in an altitude of about 1580 m);
- R is the snow-to-water ratio, estimated at 1.2 based on the water equivalent values proposed by EAWS (European Avalanche Warning Services, https://www.avalanches.org/glossary/)

The following table presents recalculated data based on the adopted corrections to obtain a more

accurate estimate of snow depth in release areas for potential avalanche triggering.

Table 5-13 Increased snow depth calculated with the coefficient k

Year	Start Date	End Date	Snow depth (cm)	Snow increase (cm)	Total snow depth (cm)
1976	February 11	February 16	93	16,9	109,9
1984	February 22	February 27	97	11,5	108,5
1987	January 11	January 16	96	10,4	106,4
1999	February 6	February 11	101	7,3	108,3
2013	February 20	February 25	72	7,6	79,6

5.3 RAMMS: Model Calibration, Simulations, and Outputs

5.3.1 Simulation Preparation

The implementation of the model requires the input of key parameters, such as slope topography, release areas, average depth of the detached snowpack, snow density ρ and friction coefficients μ and ξ. The topography of the study area was reconstructed using a high-resolution (1m x 1m) digital terrain model provided by ZRC SAZU.

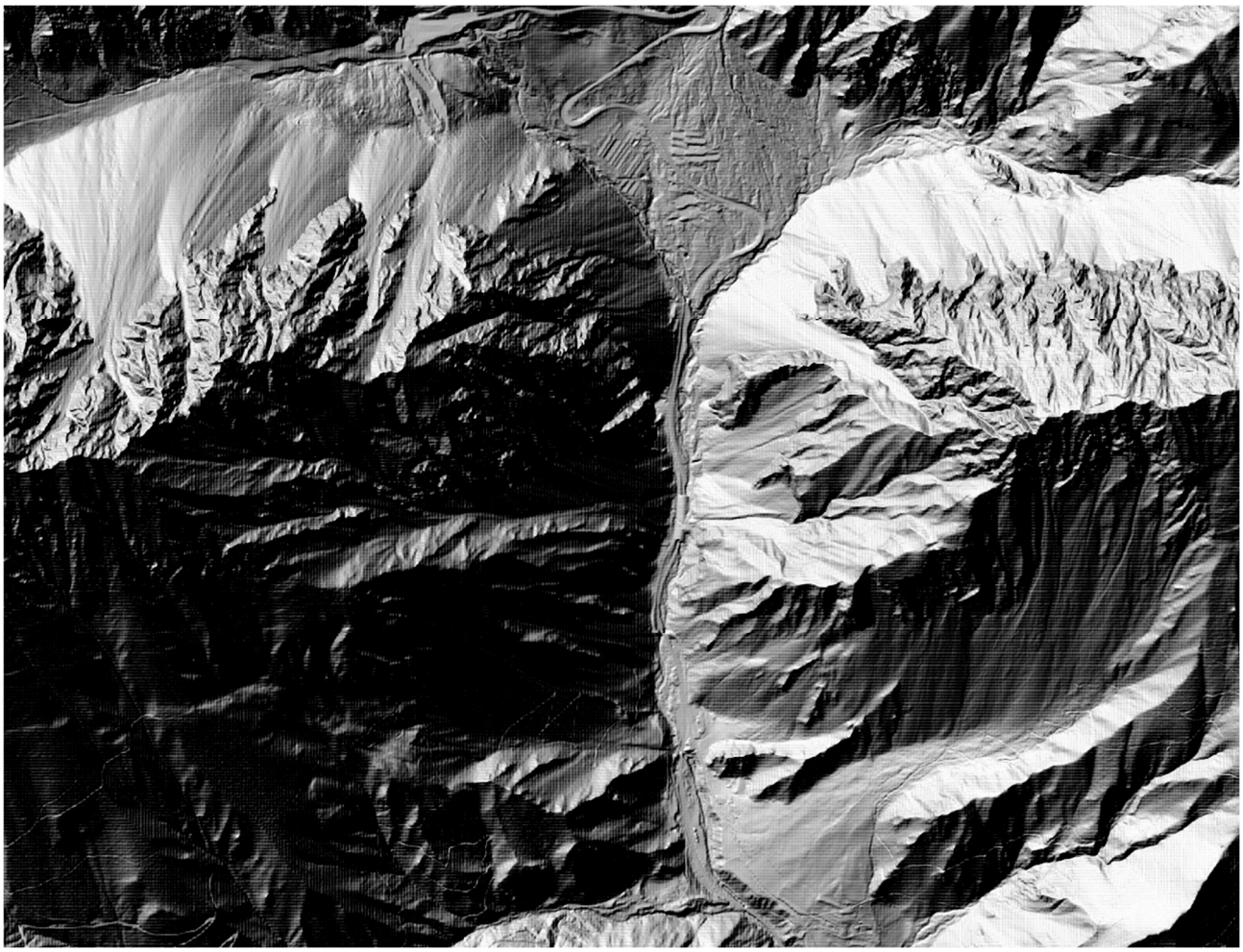

Figure 5-22 The DTM used (source: ZRC SAZU, Mauro Hrvatin)

The release areas were imported into the model as shapefiles but can also be drawn directly on the DTM using the Draw function in RAMMS.

To optimize computational performance, the calculation domain was restricted to the area of interest, corresponding to the avalanche path.

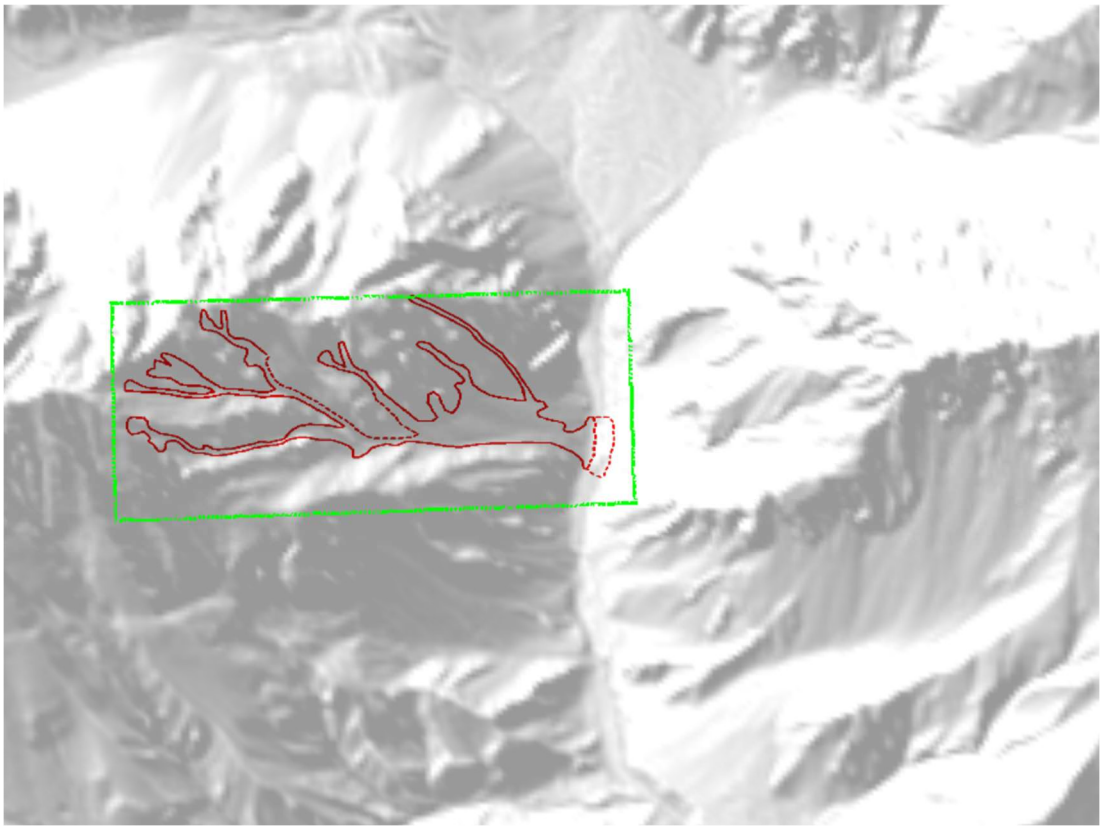

Figure 5-23 The calculation domain outlined in green

The vegetation height data at the study site was integrated into the model using an ASCII file, also provided by ZRC SAZU.

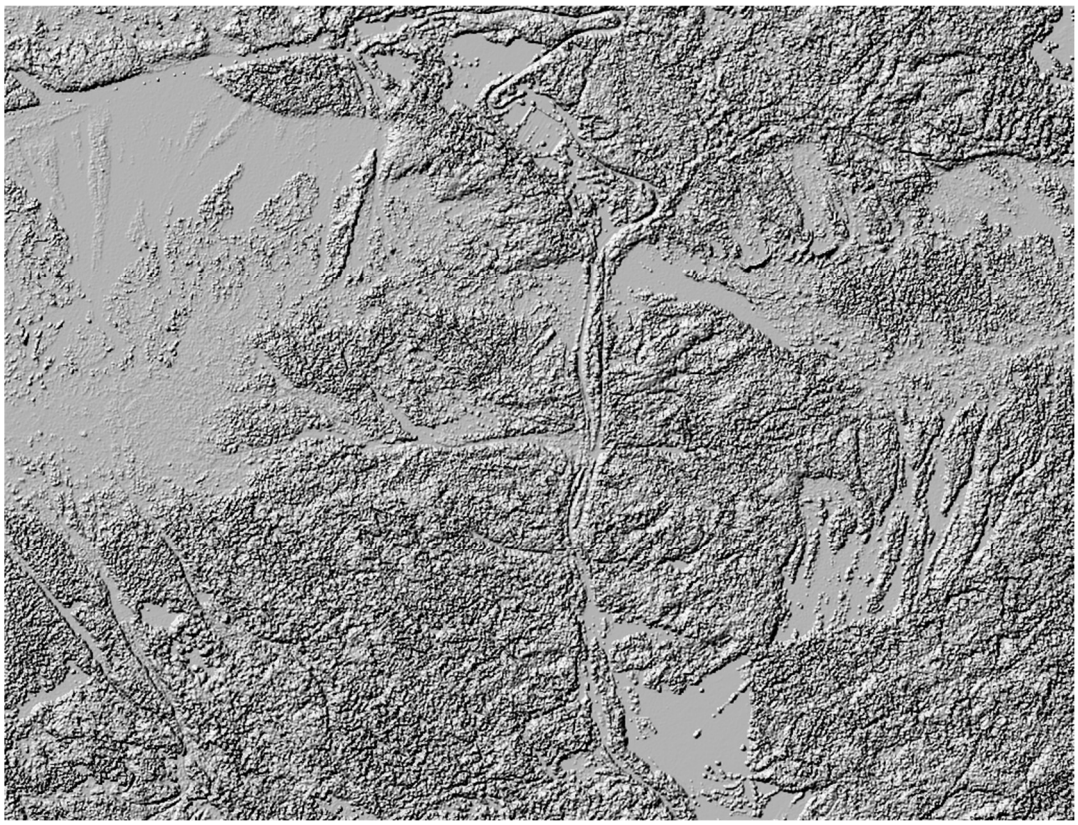

Figure 5-24 The forest file displayed with hillshade (source: ZRC SAZU, Mauro Hrvatin)

Friction parameters were assigned through the Mu/Xi File, based on a 30-year avalanche return period.

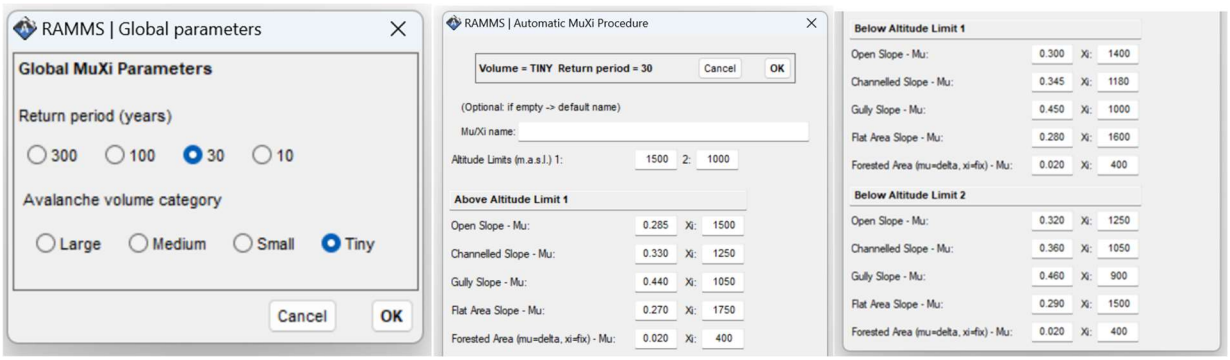

Figure 5-25 Global Parameters and Automatic MuXi Procedure

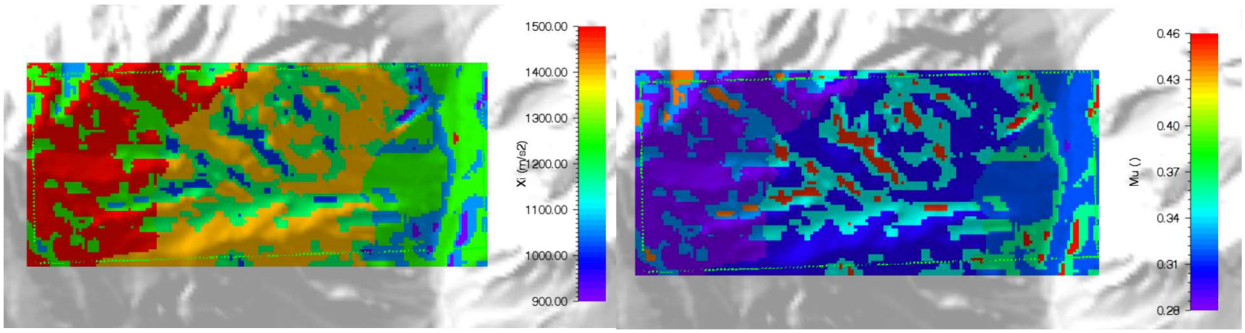

Figure 5-26 Automatic MuXi Procedure output. Left: Xi. Right: Mu.

The volume of the detached snow mass is automatically determined by the RAMMS::AVALANCHE model, combining the extent of the release areas with the average snowpack depth.

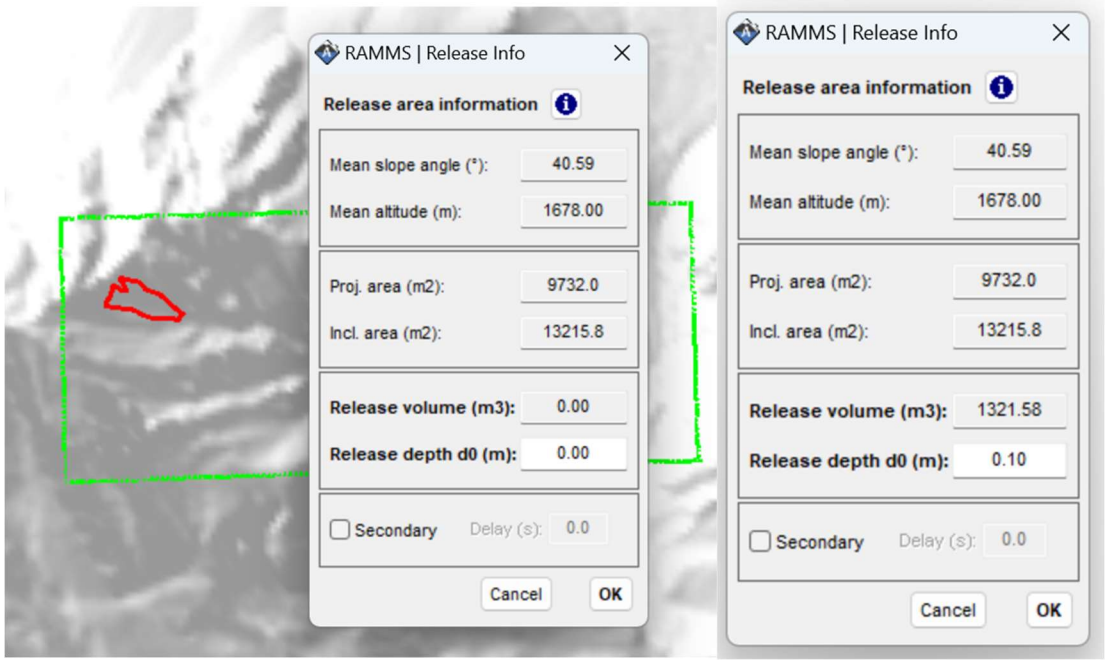

Figure 5-27 Release info and release volume

The snow density value was set at 300 kg/m³, following Dent & Lang (1982) and McClung & Schaerer (2006). Snow density plays a crucial role in calculating simulated pressures; however, this parameter is not analysed in this thesis. Snow cohesion was kept constant at 50 kPa, as recommended by the software manual.

During the avalanche event simulations, the effect of terrain curvature was included in the model, and for all conducted simulations, a uniform simulation time of 300 seconds was set. The total moment limit percentage required to conclude the calculation was set at 5%, in accordance with best practices in dynamic simulation.

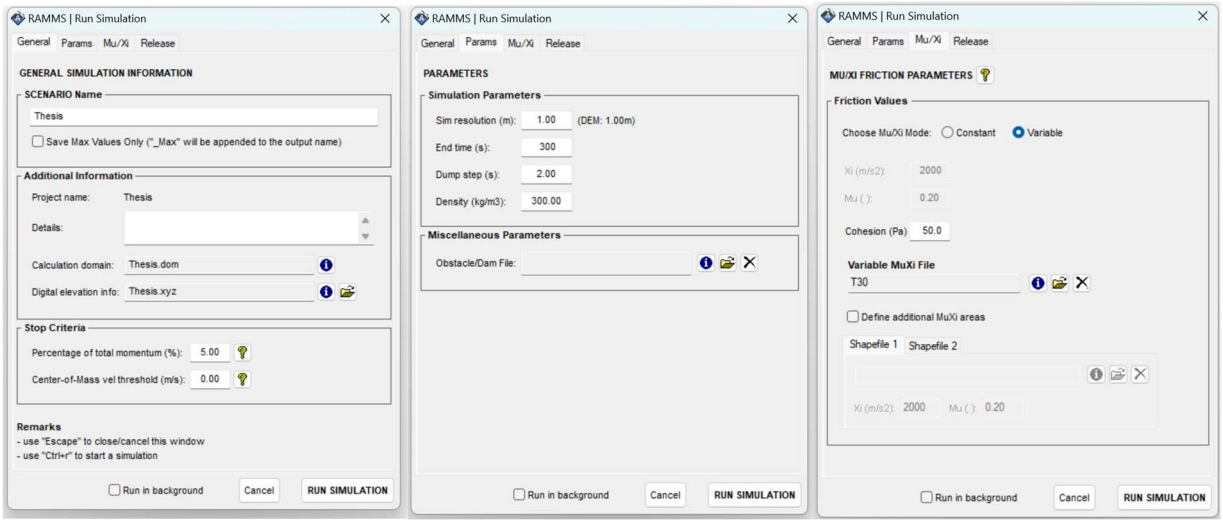

Figure 5-28 Run Simulation

Several simulation experiments were conducted, and the results were carefully analysed. Notably, during a simulation with a simultaneous detachment of 0.40 m from all potential trigger zones, the software was observed to accurately reproduce the avalanche path, indicating that the model was appropriately calibrated.

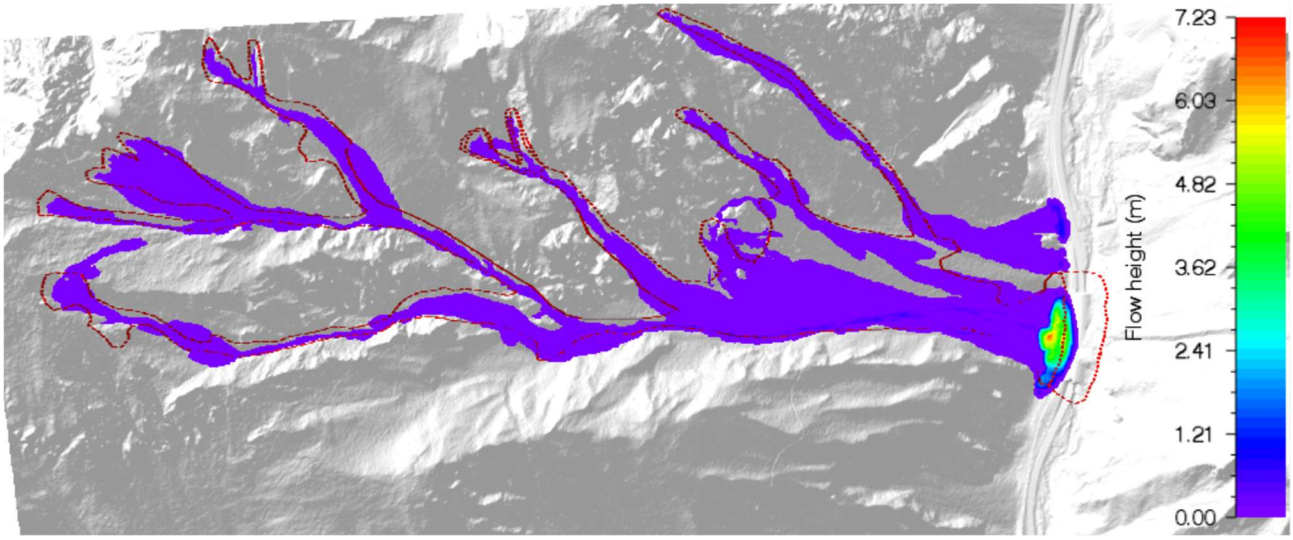

Figure 5-29 First simulation from all potential breakaway zones (Snow depth = 0.40m)

5.3.2 Simulations and Output

The simulations were carried out to confirm the necessity of the tunnel in mitigating risks for road users. While the importance of the structure was visually evident, the simulations provided irrefutable confirmation, validating initial hypotheses.

Detachment zone number 3 was selected, and simulations were conducted varying the snow depth at detachment in 5 cm increments, starting from an initial value of 10 cm. Three simulations were required to reach a detachment height of 20 cm, with a total detached snow volume of 2643.17 m^3. This quantity represents the volume of snow that, in the absence of the tunnel, would interfere with the road, increasing road safety risks.

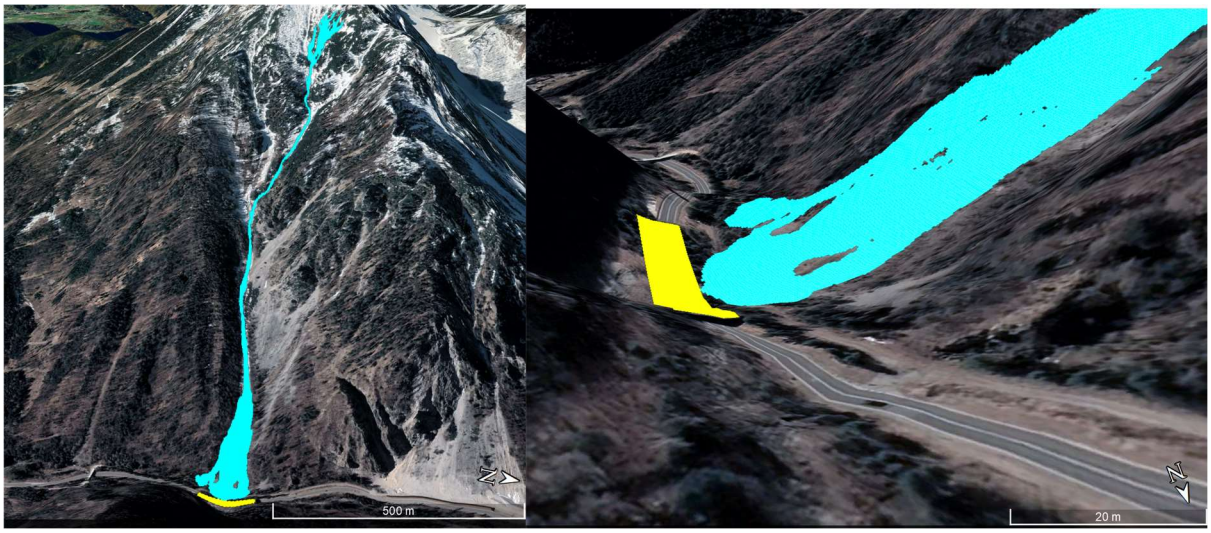

Figure 5-30 Simulation without the tunnel shown in Google Earth (Snow depth = 0.20m)

A 16,071-day analysis period (1976–2019) was considered, covering all seasons, during which 1,551 days recorded more than 20 cm of snow on the ground. Detailed analysis of the December–April period, covering 96% of avalanche triggers in Slovenia (Volk Bahun, 2020), showed that 1,548 days out of 6,710 (over 23% of the total) had accumulations exceeding 20 cm of snow. Although snow accumulation is not the sole determinant of avalanche triggering, these results reinforce the tunnel's importance as a protective measure.

Based on previous data and potential inconsistencies in data (Lendvai et al., 2015), numerous simulations were performed varying detachment heights between 60 cm and 110 cm, increasing the detachment height in 10 cm increments, and analysing interactions with the tunnel and road. Given the greater detachment height, optimal inclination and curvature, and lack of vegetation, avalanches were simulated in detachment zones 1, 2, 3, and 4, excluding zones 5, 6, 7, and 8.

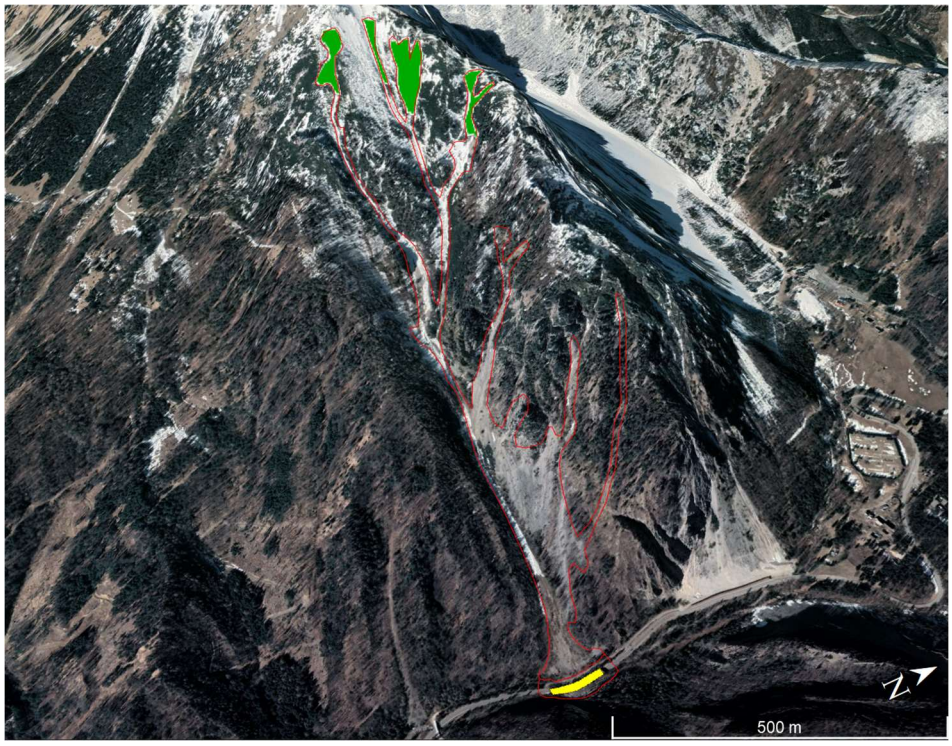

Figure 5-31 In green, the considered release zones (1, 2, 3, and 4). In yellow, the tunnel. The red line represents the avalanche track

Since it is not possible to define snow cover presence on the ground and subsequent erosion due to avalanche action, the software only simulates the movement of detached snow volume along the channel until reaching the tunnel. The simulations were conducted separately for each snow depth value and detachment area. It was found that no single detachment, ranging from 0.60 m to 1.10 m, was sufficient to interfere with the road. Additionally, even considering the largest release area, approximately 1.67 m of snow was required to generate interference between the avalanche and the road.

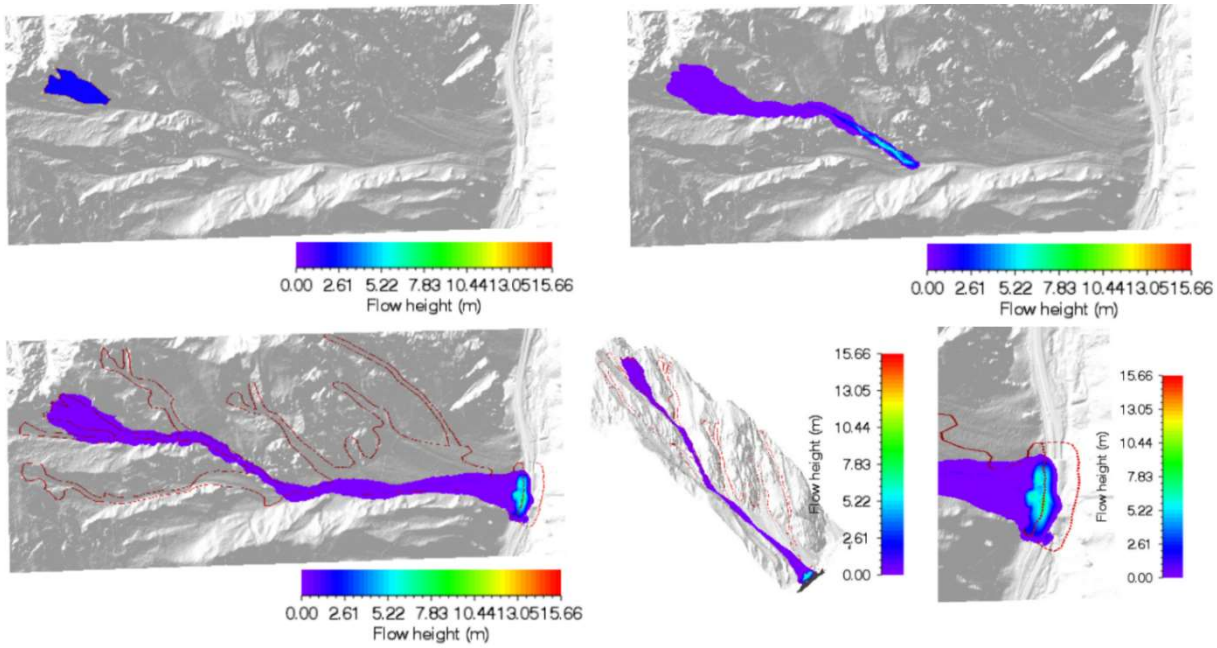

Figure 5-32 Release area number 3 (Snow depth = 1.67m)

In the analysis, it was considered that triggering an avalanche in one release area induces instability in adjacent areas, removing the foot of each area and increasing the risk of successive avalanches. Various scenarios were simulated where two or more detachments occurred consecutively or overlapped, simulating cases where an avalanche accumulates on the deposit left by a previous avalanche. The simulations indicated that at least two detachments, with snow depth between 0.60 and 1.10 m, occurring consecutively or overlapping, were sufficient to cause interference between the avalanche and the road.

Ignoring velocity and pressure and considering only snow height, it was observed that detachment order does not influence the total snow volume, implying no significant variations in deposits when reversing detachment orders (e.g., 1+2 is equivalent to 2+1).

The constant and variable parameters in each simulation are as follows:

Table 5-14 Summary table of constant parameters and variable parameters used in the simulations

Constant Parameters	**Parameter**	**Value**
Simulation Parameters		
	Resolution (m)	1x1
	End time (s)	300
	Dump step (s)	2
	Snow density (kg/m³)	300
Friction Parameters		
	Snow cohesion (kPa)	50
	Mu/Xi parameters	Figure 5-25
	Return Period (years)	30
Stop Criteria		
	Percentage of total moment (%)	5
	Center-of-mass velocity threshold (m/s)	0
Variable Parameters	**Parameter**	**Value**
Release Parameters		
	Snow Depth (m)	0,6 - 1,1
	Volume (m³)	Calculated by RAMMS
	Avalanche Volume Category	Calculated by RAMMS

Two Releases:

- With a snow depth of 1.1 m, the most critical scenario corresponds to the combined release of zones 1 and 3. A moderate scenario, which still results in snow reaching the roadway, is observed in the case of the combined release of zones 3 and 4. No interference with the roadway is detected for other release combinations: 1+2, 1+4, 2+3, and 2+4.
- With a snow depth of 1.0 m, the only scenario leading to interference with the roadway is the combined release of zones 1 and 3. For snow depths below 1.0 m, no interference with the roadway is observed for any two-release combinations.

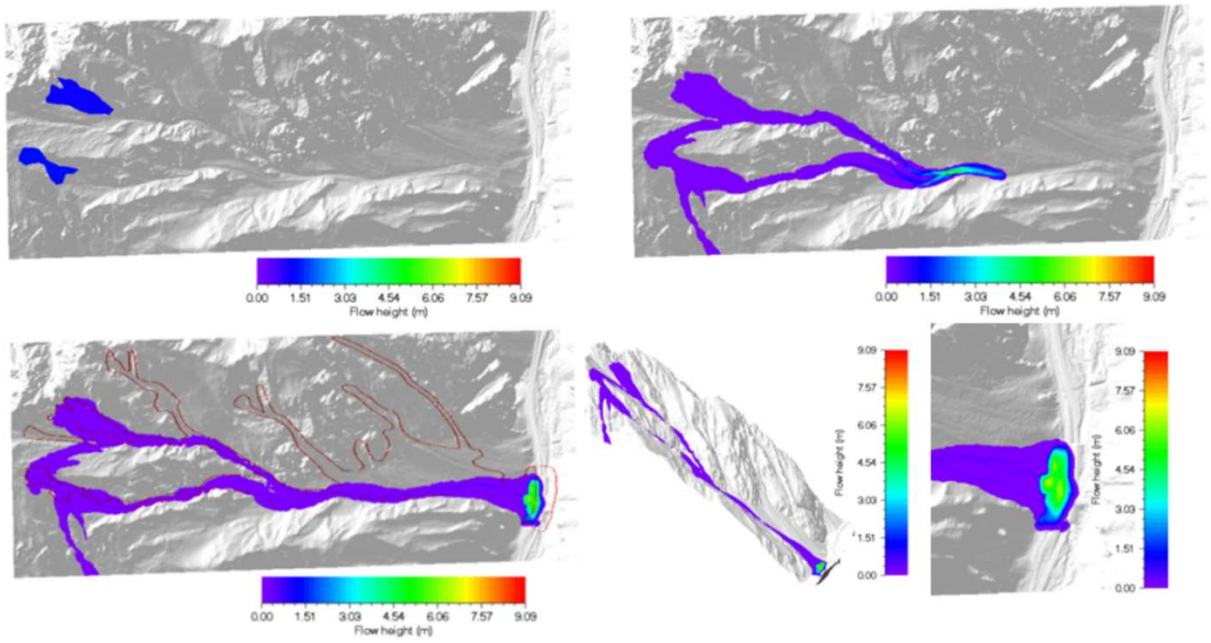

Figure 5-33 Release areas number 1 and 3 (Snow depth = 1.00m)

Three Releases:

- With a snow depth of 1.1 m, only the combination 1+2+4 does not result in interference with the roadway; all other configurations lead to interference.
- With a snow depth of 1.0 m, the same pattern is observed as for the 1.1 m scenario, with only the combination 1+2+4 preventing roadway interference.
- With a snow depth of 0.90 m, no interference is observed for the combinations 1+2+4 and 2+3+4.

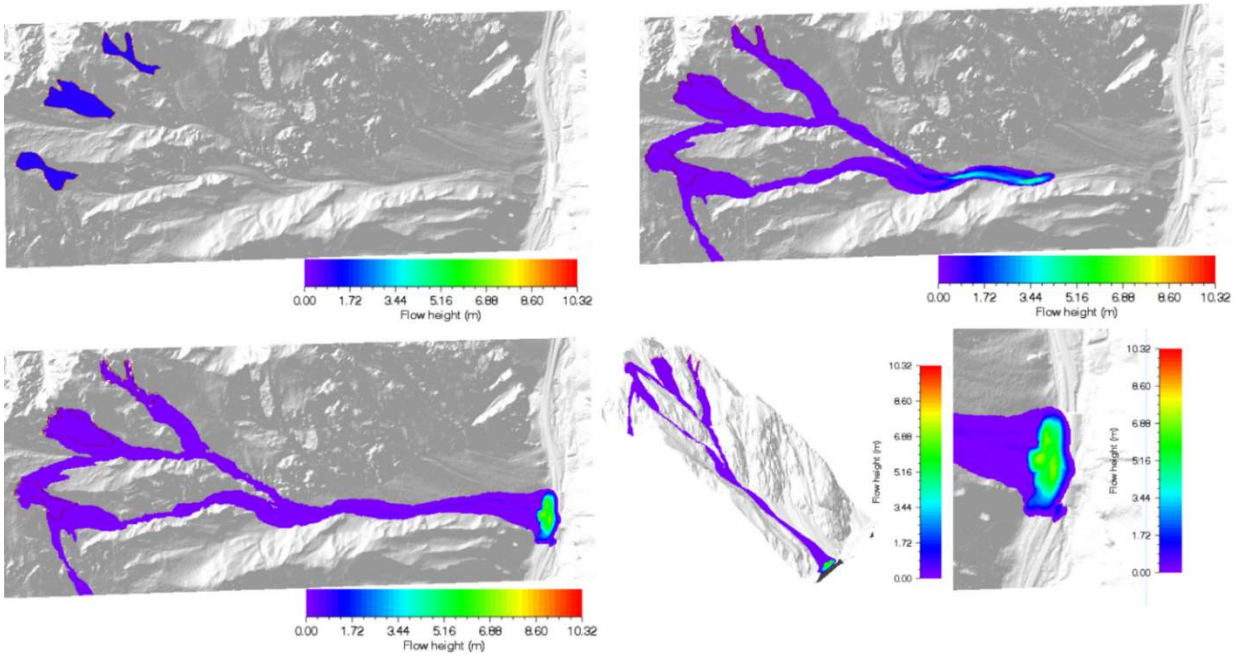

Figure 5-34 Release areas number 1, 3 and 4 (Snow depth = 0.90m)

- With a snow depth of 0.80 m, the combination 1+2+3 also does not result in roadway interference.
- With a snow depth of 0.70 m, no combination leads to interference, whereas the most critical scenario (1+3+4) results in minimal interference with the roadway, occurring at a release depth of 0.77 m.

Four Releases:

- With a snow depth of 1.1 m, interference with the roadway occurs, representing the most critical scenario analysed. Equivalent scenarios with higher snow depths are considered more critical. This scenario is used as the basis for calculating the spatiotemporal probability of impact with vehicles.

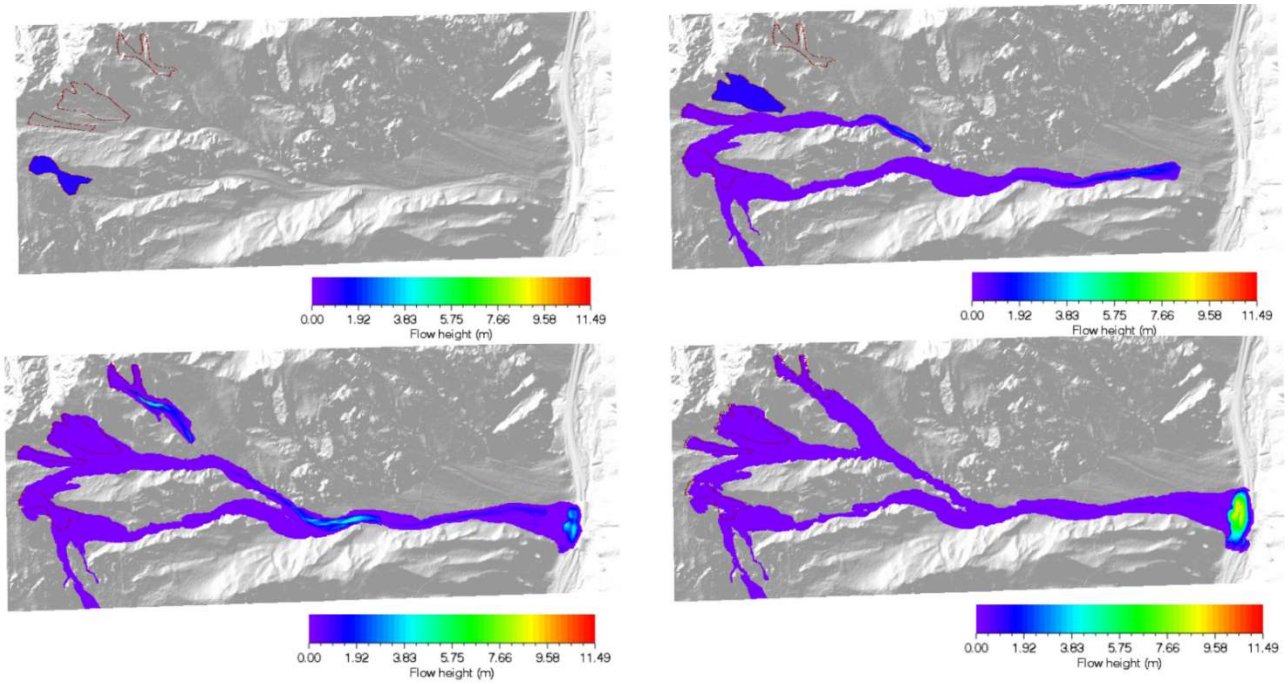

Figure 5-35 Release areas number 1, 2, 3 and 4. The releases were not simultaneous in order to simulate several overlapping avalanches triggered at different times.

- With a snow depth of 1.0 m, roadway interference is confirmed.
- With a snow depth of 0.90 m, roadway interference persists.
- With a snow depth of 0.80 m, roadway interference remains present.
- With a snow depth of 0.70 m, minimal interference is observed.
- With a snow depth of 0.60 m, no interference with the roadway occurs.

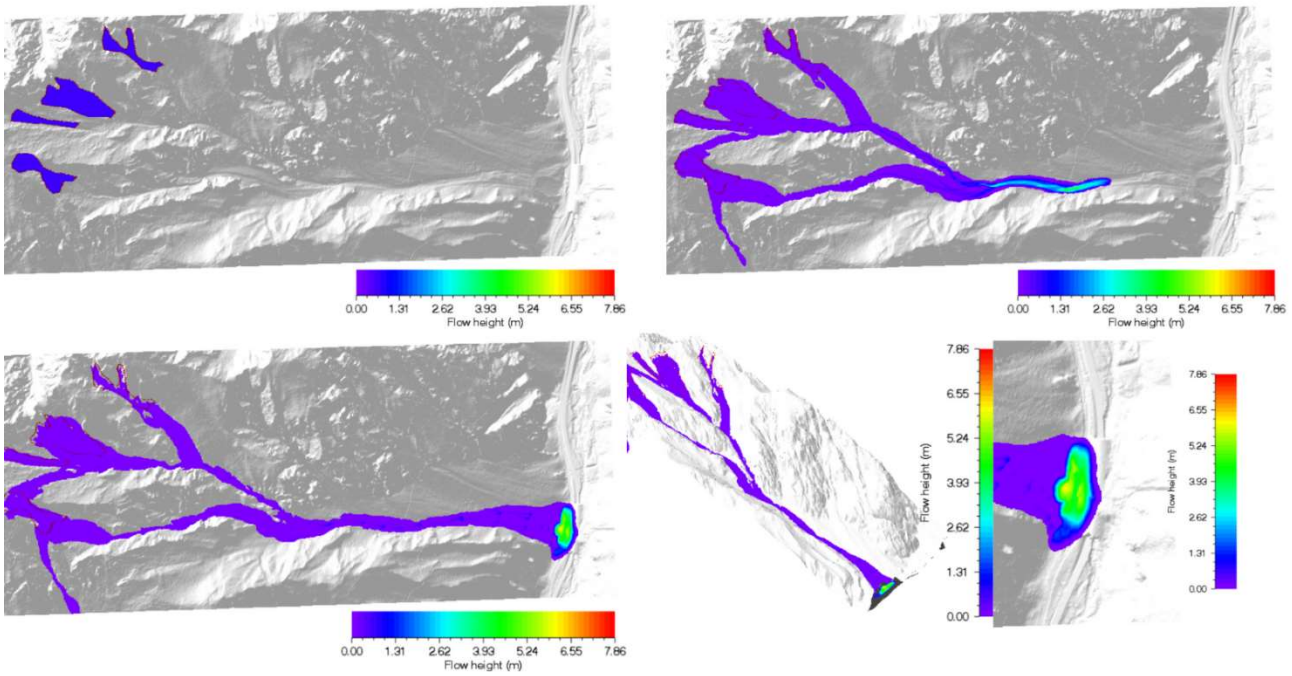

Figure 5-36 Release areas 1,2,3 and 4 (Snow depth 0.60m). No interference between avalanche and road

The minimum snow depth at which four releases can interact with the roadway is determined to be 0.68 m.

Should the reconstruction of the tunnel be necessary, it is recommended to extend its length to at least 180 meters, with an additional extension of approximately 25 meters both upstream and downstream of the current structure.

5.4 Avalanche Damage Analysis on the Road Network

5.4.1 Spatio-temporal Impact Probability

The interaction between avalanche phenomena and road networks represents one of the main challenges in mountainous areas. Avalanches can cause significant disruptions to traffic flow or, in the worst cases, direct damage to vehicles, resulting in injuries or fatalities. Assessing the probability of such an impact provides critical insights into the associated avalanche risk and the necessity of implementing preventive measures.

According to a study conducted on avalanches in France, the primary form of damage is road obstruction, which accounts for at least 69.5% of recorded damaging events. Material damage to additional infrastructures, attached equipment, and vehicles represents significantly lower percentages, specifically 5%, 1.7%, and 1.5%, respectively. Direct damage to the road itself accounts for a modest 0.7% (Leone et al., 2014).

To calculate the spatiotemporal probability (PST) of a direct impact between a vehicle and the falling snow mass, a model was used to simulate the avalanche's maximum reach, assuming four snow releases of 1.1 m, with a total volume exceeding 35,000 m³. The employed equation is based on the method proposed by Roberds (2005) and considers various factors, including the likelihood of frontal and lateral impacts, the velocity of both the vehicle and the falling mass, as well as the dimensions of both the vehicle and the avalanche mass.

The equation used to calculate the spatiotemporal probability of impact (PST) is as follows:

$$P_{ST} = 1 - \frac{[L_S - (\mathrm{L_E} + \mathrm{W_V}) * \frac{\mathrm{V_V}}{\mathrm{V_E}}] - W_E}{\mathrm{L_S} + \mathrm{L_V}}$$

Where:

- P_{ST} is the spatiotemporal probability of impact between the vehicle and the falling mass, expressed as a dimensionless value.
- L_S is the distance between vehicles, measured in meters, assuming a uniform distribution of vehicles on the road. To estimate the distance between vehicles, the average number of vehicles per day was used. This data was obtained from ODPRTI PODATKI SLOVENIJE (at https://podatki.gov.si/dataset/pldp-karte-prometnih-obremenitev).

Table 5-15 Number of vehicles per day

Štev. ceste	Prometni odsek	Stac. začetka	Stac. konca	Motorji	Osebna vozila	Avto busi	Lah. tov. < 3,5t	Sr. tov. 3,5-7t	Tež. tov. nad 7t
Road number	*Traffic section*	*Starting station*	*Ending station*	*Motor cycles*	*Cars*	*Buses*	*Light trucks < 3.5t*	*Medium trucks 3.5-7t*	*Heavy trucks over 7t*
101	MP LJUBELJ - BISTRICA (TRŽIČ)	0	12,5	123	2.102	8	244	6	1

- L_E is the length of the falling mass, perpendicular to the vehicle's length, measured in meters. A value of 8 metres was used.
- W_V is the width of the vehicle, expressed in meters.

Table 5-16 Average width for each vehicle category W_V

Vehicle	Wv
Motorcycles	0,8
Cars	1,8
Buses	2,55
Light trucks < 3.5t	2,2
Medium trucks 3.5-7t	2,55
Heavy trucks over 7t	2,55

- V_V is the vehicle speed, measured in km/h. The speed limit on the G02 road is set at 70 km/h. For light vehicles (cars, motorcycles, small trucks), a constant speed of 70 km/h was assumed, whereas for larger vehicles, an average speed of 50 km/h was considered due to the presence of curves and slopes on the road.
- V_E is the velocity of the falling mass, which can reach a maximum of 21.6 km/h, as calculated using RAMMS software.
- W_E is the width of the falling mass, measured in meters. Only the width of the snow body extending downstream of the tunnel was considered. A value of 25 metres was used.
- L_V is the vehicle length, expressed in meters, estimated based on the average dimensions of each vehicle type.

Table 5-17 Average length for each vehicle category L_V

Vehicle	Lv
Motorcycles	2
Cars	4,5
Buses	12,5
Light trucks < 3.5t	5,5
Medium trucks 3.5-7t	7
Heavy trucks over 7t	11

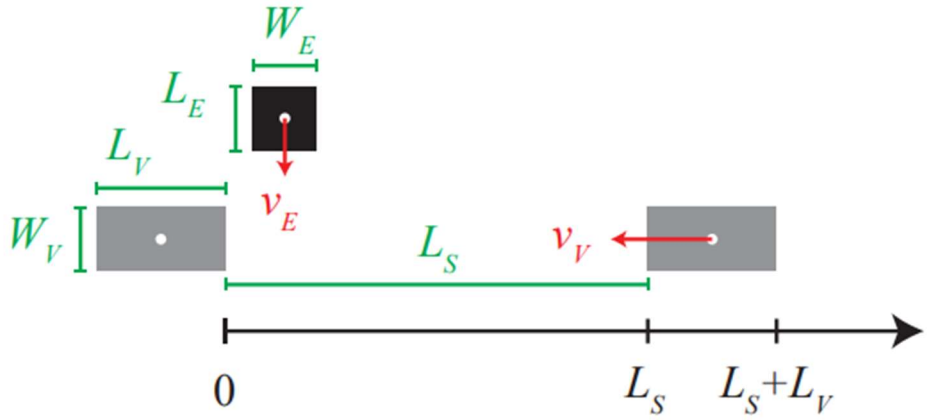

Figure 5-37 Parameters of the cars (in grey) and the falling mass (in black) used for the calculations in Roberds's (2005) method. The origin of the abscissa axis is located at the rear of the front car (Source: Nicolet et al., 2015)

The equation initially calculates the time required for the falling mass to fully traverse the vehicle's trajectory, considering its width (W_E), length (L_E), and velocity (V_E). This time is then used to determine the distance traveled by the vehicle during the time taken by the snow mass to cross.

The term $LS - \frac{(\mathrm{LE} + \mathrm{WV}) * \mathrm{vV}}{\mathrm{vE}} - WE$ represents the distance that the falling mass can cover without striking a vehicle, considering the space between vehicles and the distance traveled by the vehicle during the time interval.

The term $L_s + L_V$ represents the total distance, the sum of the space between two vehicles and the length of the vehicle itself. Finally, the probability of impact is obtained by subtracting the computed value from the total distance, yielding the probability of direct impact.

It should be noted that this equation assumes a uniform distribution of vehicles along the road, a condition that does not reflect real-world conditions. Variations in vehicle spacing (L_S) can significantly affect the probability of impact: if the spacing between vehicles is not constant, the actual impact probability may be higher than the calculated value. This is because a negative variation in L_S) (a reduction in vehicle spacing) results in a greater absolute increase in P_{ST} than the absolute reduction in P_{ST} resulting from an equivalent increase in L_S).

Furthermore, the equation only considers impact with the falling mass, without accounting for potential damage caused by the deposited material on the road after the avalanche event. However, depending on the avalanche type and speed, the falling mass may involve a large volume of snow and persist over a longer duration, further complicating the hazard assessment. This aspect is particularly relevant for large vehicles such as trucks and trains, which have limited manoeuvrability to avoid obstacles and restricted braking distances.

For each vehicle type, the spatiotemporal probability (P_{ST}) of impact was calculated and subsequently weighted to obtain an overall probability value. Calculations were performed daily for the year 2023, considering 24-hour traffic data, yielding an initial result:

$$P_{ST} = 0{,}0656$$

Subsequently, it was considered that most of the traffic flow occurs during the 12 daytime hours (from 7:00 AM to 7:00 PM). In the worst-case scenario, where all vehicles transit during these 12 hours, the probability of impact doubles:

$$P_{ST} = 0{,}1305$$

For a more realistic estimate, it was assumed that only 80% of vehicles travel during daylight hours and that motorcycle transit is nearly negligible during the winter season, especially in cases of heavy snowfall. Recalculating the probability with these parameters yielded an intermediate value that more accurately reflects actual traffic conditions. In this case:

$$P_{ST} = 0{,}1097$$

Based on the available sources and various considerations, it is possible to estimate a return period of 30 years for the case study avalanche. Using this data, the probability that a vehicle will be struck by an avalanche within a single year is calculated to be 0.365%.

$$P_{1y} = 0{,}1097 * \frac{1}{30} = 3{,}65 * 10^{-3}$$

5.4.2 Mortality Risk Assessment

Following the previous analysis, an assessment of the fatality risk for individuals trapped inside their vehicles due to an avalanche impact on the roadway was conducted. This analysis was performed in accordance with the guidelines regarding natural hazards along national roads (ASTRA, 2012) which states that the individual risk of death in areas exposed to natural hazards must remain below 10^{-5}.

To estimate the probability of fatality, the calculation considered the product of the probability of impact (P_{1y}), the fatality rate associated with a vehicle being struck by an avalanche (F), and the average number of occupants per vehicle (N).

These parameters vary depending on the type of vehicle involved. For instance, the average number of passengers in a car is generally lower than in a bus. In the absence of specific data regarding bus types and passenger occupancy for individual trips along the studied road section, a conservative assumption was adopted, considering a single occupant per transiting vehicle ($N = 1$). The probability of impact was referenced from the previously determined value. Regarding the fatality rate within the vehicle following an avalanche impact, the study by Wilhelm (1997) was used as a reference, which indicates this value to be $F = 0{,}18$.

Thus, the probability of fatality can be calculated as follows:

$$P_F = P_{1y} * F * N = \ 3{,}65 * 10^{-3} * 0{,}18 * 1 = 6{,}57 * 10^{-4}$$

$$6{,}57 * 10^{-4} > 10^{-5}$$

The obtained value is significantly higher than the acceptable risk standards.

5.4.3 Rear-End Collision Scenario

In the analysis of the rear-end collision scenario, it was assumed that the mortality rate is comparable to that of an average highway rear-end collision, regardless of the nature and intensity of the triggering event. According to the Swiss Association of Road and Transport Professionals (VSS, 1999) , this rate (F_{R-E}) amounts to 0.0066.

To estimate the probability of a rear-end collision occurring on a specific road section, it would be necessary to examine the distribution of such events on the national road network. However, in the absence of specific data related to the study area, reference was made to an analysis conducted on the cantonal roads of the Canton of Bern, which found that, in the event of an incident, the probability of a rear-end collision (P_C) is approximately 15%. This value, being an average independent of the road type, was also adopted in the present study.

The average number (N) of people involved in the "rear-end collision" scenario is 1.76 (Gogniat, 2011). The probability of fatality resulting from this scenario is therefore calculated as follows:

$$P_{F_{R-E}} = P_{1y} * \ P_C * F_{R-E} * N = \ 3{,}65 * 10^{-3} * 0{,}15 * 0{,}0066 * 1{,}76 = 6{,}35 * 10^{-6}$$

$$6{,}35 * 10^{-6} < 10^{-5}$$

The obtained value falls within the acceptable risk limits.

6. Economic and Risk Assessment of Avalanche Impact on Road Infrastructure

6.1 Assessment of Transport Infrastructure Vulnerability

The assessment of transport infrastructure vulnerability plays a crucial role in the planning and management of road networks, especially in a context characterized by increasing uncertainty related to natural phenomena. These assessments typically employ two distinct approaches: direct and indirect.

- Direct Approach. Analysis of physical damage: The direct approach focuses on analysing the material damage that the infrastructure sustains following a critical event. Such damage includes repair or replacement costs of compromised infrastructure components and immediate losses, including injuries, fatalities, and environmental damage.
  - Fatalities: Quantifying human losses is a complex process that involves the use of economic estimates related to the value of human life. Although assigning a monetary value to life is problematic, economic assessments use the concept of "Value of a Statistical Life" (VSL), derived from studies analysing people's willingness to incur costs to reduce mortality risk (Miller, 2000).
  - Environmental Damage: Assessing environmental damage is particularly complex and requires a case-by-case analysis. The damage caused by an avalanche presents a lower magnitude compared to other phenomena that cause soil and water pollution, greenhouse gas emissions, destruction of habitats, and consequent biodiversity loss.
  - Immediate Functional Disruption of Infrastructure: The immediate disruption of infrastructure functionality following a damaging event represents a primary direct loss, as it affects mobility and connectivity in the affected areas. Unlike indirect consequences, which emerge later in the form of route or transportation mode changes, immediate disruption constitutes a direct and tangible effect of the physical damage sustained by the infrastructure.

- Indirect Approach. Analysis of network utilization consequences: The indirect approach focuses on the repercussions resulting from the inaccessibility of the damaged infrastructure, which manifest through (Erath, 2011):
  - Increased travel times and distances, as users are forced to take alternative routes, leading to longer travel times, greater total distance, and consequently higher transportation costs.
  - Changes in the choice of transportation mode, with a potential increase in the use of public transport and consequent impacts on costs, travel times, and congestion.
  - Changes in travel destinations, particularly for trips related to commercial or recreational activities, affecting traffic flows and local economic dynamics.

For a comprehensive assessment of transport infrastructure vulnerability, it is essential to integrate both methodologies. The simple algebraic sum of direct and indirect costs allows for estimating the overall impact of an infrastructure malfunction. To fully understand the impact of natural events, it would be appropriate to adopt an approach that considers both direct consequences, namely immediate physical damage, and indirect consequences, such as traffic flow disruptions and changes

in travel behaviour. Integrating these two perspectives enables a comprehensive and accurate risk assessment (Erath, 2011).

However, for the purposes of this study, certain important aspects will not be considered, such as the economic value of human losses, immediate environmental costs, and indirect economic repercussions. The evaluation will focus only on analysing the cost borne by the state for snow removal from the roadway, comparing it with the cost of constructing a protective structure suitable for the dimensions of the considered event.

6.2 Cost Estimation for the Construction of an Avalanche Protection Tunnel

The determination of the cost of constructing an avalanche protection tunnel is a crucial aspect in the planning and design of road protection infrastructure. To obtain a realistic estimate, a comparison was made between the construction costs of recently built or planned avalanche protection tunnels in various countries to identify a reference range useful for economic evaluation. Specifically, average prices observed in Italy, France, and Slovenia were analysed, considering both open protection galleries (protection roofs) and complete road tunnels, characterized by greater structural and engineering complexity.

For the Italian context, data provided by the Autonomous Province of Bolzano, one of the areas most exposed to avalanche risk and with extensive experience in constructing protective infrastructure, were examined. Some significant examples include:

- Passo Giovo (completed in 2018): Construction of a simple gallery (protection roof) 180 meters long, with a total cost of 3.1 million euros, corresponding to approximately €17,200 per linear meter.

Figure 6-1 Avalanche tunnel Passo Giovo, Italy. (Source: Provincia Autonoma di Bolzano)

- Lappago (completed in 2014): Construction of a complete road tunnel 175 meters long, with a total cost of 5 million euros, equivalent to €28,600/m.
- Vernago (approved project in 2024): The project involves an open gallery 325 meters long, with an estimated cost of about 12 million euros, or €36,900/m.

- Rio Bianco (completed in 2024): Construction of a 264-meter-long gallery. Of these, 170 meters will be an open gallery, while the remaining 94 meters will be a fully enclosed road tunnel. The total cost of the project was 6.9 million euros, with an average cost calculated between the two types of structures amounting to €26,100/m.

In Austria, the avalanche protection tunnel constructed in Nauders serves as a notable example. This structure features a protective roof tunnel, or open gallery, which connects to a natural rock tunnel. The tunnel spans 320 meters, with a construction cost of €6.9 million, equating to €21,500 per meter.

Figure 6-2 Left: Nuders gallery portal. Right: Connection of gallery structure with natural tunnel. (Source: PORR AG)

In France, a particularly significant project is currently under construction in the Pyrenees, in the municipality of L'Hospitalet-près-l'Andorre. The project, initiated in May 2024, involves the construction of a 300-meter-long avalanche protection tunnel, with a total investment of 24 million euros, resulting in an estimated average cost of €80,000/m.

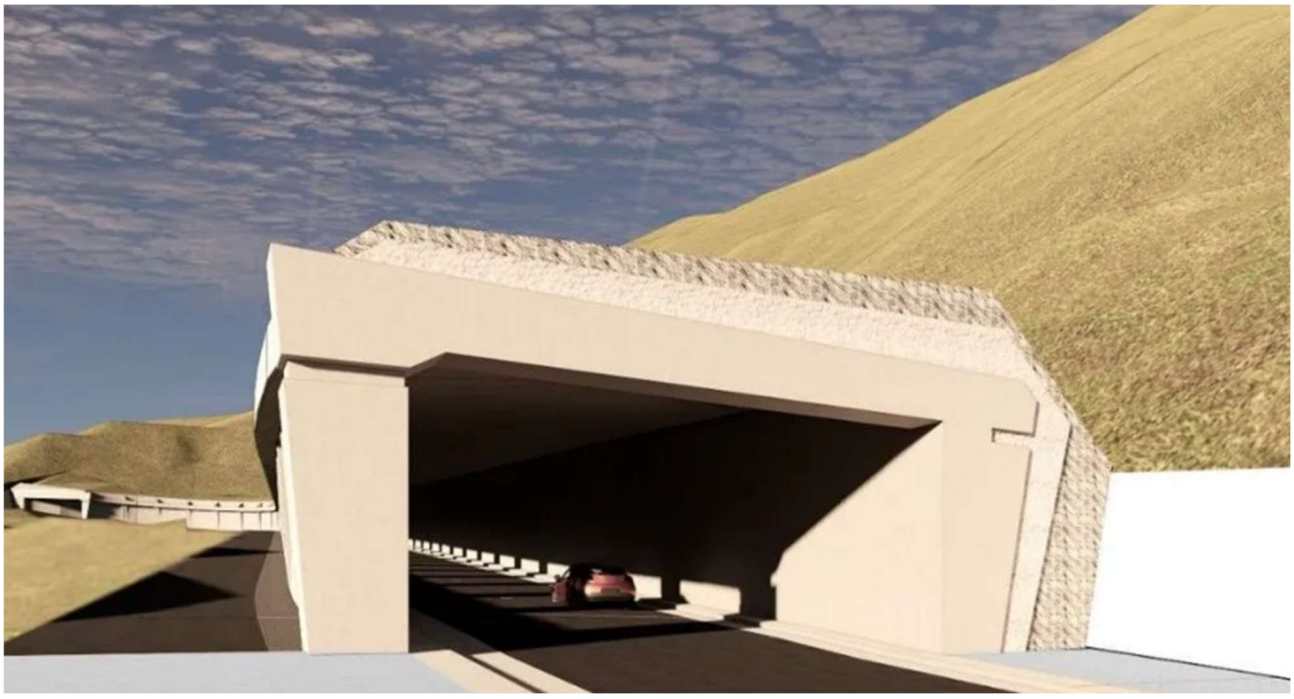

Figure 6-3 Artistic vision of the future avalanche tunnel on the RN 320 - DR towards Andorra. (Source: ICI, Francois David)

Estimated Costs for Avalanche Protection Tunnels in Slovenia

Regarding Slovenia, the available data indicate the following cost ranges:

- Simple open galleries (protection roofs): Between €10,000 and €20,000/m.

  For a hypothetical length of 180 meters, the estimated investment would range between 1.8 and 3.6 million euros.

- Complete road tunnels: Between €30,000 and €50,000/m, with potential higher costs depending on geological and construction conditions.

  For a 180-meter-long tunnel, the estimated expenditure ranges between 5.4 and 9 million euros.

Considering the construction costs of an avalanche protection tunnel, it is essential to highlight the technical and economic challenges that may arise during the development of similar infrastructures. A significant example is the Šklendrovec tunnel project in Slovenia, as reported in an article by the newspaper *Delo* on February 17, 2025.

Originally scheduled for completion in June 2023, the tunnel experienced significant delays due to unforeseen geological conditions, which necessitated structural modifications and additional interventions to ensure the stability of the structure. The discovery of a different soil composition than initially indicated in the project documentation required supplementary investigations and the implementation of solutions such as the use of pillars, anchors, and reinforcement walls. Additionally, the identification of a fracture in the ground led to further studies and stabilization measures.

These complications had a substantial impact on costs: the initial budget for the 300-meter-long tunnel was €6.4 million (€21,300/m), but it progressively increased to €10 million (€33,300/m), partly due to inflation and contractual price adjustments.

Despite the crucial role of structural defense works in mitigating natural hazards, the case of the Šklendrovec tunnel illustrates how tunnel construction is subject to uncertainties and unforeseen challenges that affect both completion timelines and final costs.

7. Conclusions

This study addresses the issue of avalanche risk in relation to transport infrastructure by adopting a multidisciplinary approach that integrates snowpack analysis, numerical modelling, economic evaluation of protective measures, and risk quantification. The primary objective was to analyse the interaction between avalanche phenomena and road infrastructure, with particular attention to the Podljubelj avalanche protection tunnel. To this end, the RAMMS Avalanche software was employed, enabling the simulation of various snow detachment and flow scenarios, which provided the foundation for risk assessment.

The results highlight that the amount of snow present in the detachment zone is a key factor in determining the avalanche's runout distance. Under specific conditions, the snow mass can reach the roadway, significantly increasing the risk of vehicles being blocked or impacted by the avalanche. The subsequent risk calculation, applied to road user safety, provided a general indication of the necessity of the existing tunnel. Although the calculated risk level was found to be high, the analysis confirmed the tunnel's effectiveness in mitigating the hazard: in the absence of such infrastructure, the risk level would be considerably higher.

However, the analysis encountered certain critical issues, primarily due to the lack of an avalanche cadastre. Snow depth estimation was conducted based on climatic and precipitation data, introducing inevitable margins of uncertainty. Furthermore, the simulations performed using RAMMS did not account for the phenomenon of snow erosion, which could significantly increase the initial avalanche volume, nor for variations in speed and cohesion within the flow. Finally, the risk calculation was necessarily subject to assumptions and simplifications, particularly regarding vehicle spacing and the hourly distribution of traffic along the analysed road section.

To mitigate avalanche risk, various infrastructural solutions can be considered, evaluating their effectiveness and economic sustainability. Among these, the construction of a new protection tunnel would represent the safest option, as it would provide complete protection for vehicles in transit, eliminating any possibility of direct impact with the snow mass. However, such an intervention would entail extremely high costs, which may not be justified given current snow conditions and uncertainties related to climate change. Additionally, the construction of such large-scale infrastructure could face technical and economic challenges, with the risk of further increasing already considerable costs.

In light of these considerations, it may be appropriate to also evaluate alternative solutions to complement the existing tunnel, considering both active and passive protective measures aimed at reducing the energy and extent of avalanches before they reach the roadway, as initially proposed in the first project. In the detachment zone, the use of snow nets, avalanche barriers, and snow bridges could help prevent or limit snow mass detachment. In the runout zone, mitigation structures such as wedges, deflectors, and braking mounds could reduce avalanche velocity and dissipate its energy, thereby decreasing both the runout distance and destructive potential. Although these solutions

generally involve lower costs compared to building a new tunnel, their effectiveness depends on careful design—which was not assessed in this study—and regular maintenance to ensure long-term functionality.
Beyond the structural works, considering the results of the analysis carried out in this thesis, it is suggested to seriously consider temporary defence measures such as artificial avalanche triggering, which, both in terms of operability and economics, seems to be the better solution in case of critical avalanches (for the tunnel) and multiple events.

To improve avalanche risk management in the long term, it is essential to adopt an integrated approach that combines modelling, real-time monitoring, and targeted structural interventions. Furthermore, the development of remote sensing technologies and the application of artificial intelligence algorithms could, in the future, significantly enhance the accuracy of avalanche forecasting, enabling more timely and effective preventive measures.

In conclusion, any mitigation strategy must be based on a thorough cost-benefit analysis, considering not only the level of protection offered by different solutions but also their economic and environmental sustainability. A multidisciplinary approach that integrates engineering, snow science, and economic expertise is essential to effectively address the challenges posed by avalanche risk in mountainous regions.

8. References

Associazione svizzera dei professionisti della strada e dei trasporti VSS (1999). *Strassenverkehrsunfälle – Unfallzahlen, Unfallstatistiken, Unfallkosten*, SN640 007.

ASTRA 89001 (2012). *Pericoli naturali lungo le strade nazionali: gestione dei rischi*.

ASTRA/Federal Roads Office. (2007). *Einwirkungen infolge Lawinen auf Schutzgalerien*. Bern.

Bakkehoi, S., Domaas, U., Lied, K. (1983). Calculation of Snow Avalanche Runout Distance. *Annals of Glaciology*, 4, 24-29. DOI: https://doi.org/10.3189/S0260305500005188

Barbolini, M. (2004). *Modelli per il calcolo delle valanghe*. Università degli Studi di Pavia, Dip. Ing. Idraulica e Ambientale.

Bebi, P., Kulakowski, D. e Rixen, C. (2009). Snow avalanche disturbances in forest ecosystems—State of research and implications for management. *Forest Ecology and Management*.

Brignolo, I. (2020). *Piene di progetto nei bacini alpini: evidenze empiriche e modellazione su base geomorfoclimatica* [Tesi di laurea magistrale]. Politecnico di Torino, Torino, Italia.

Bühler, C. e Swiss Federal Institute for Forest, Snow and Landscape Research (WSL). (2014). *RAMMS - Rapid Mass Movement Simulations Manual*.

Ceresetti, D. (2006). Analisi delle precipitazioni. In *Bacino del T. Cenischia: Valutazione delle Problematiche Idrologiche e Idrauliche* (pp. 68-70).

Chiaia, B. e Frigo, B. (2024). *Linee guida per la valutazione e la mitigazione del rischio valanghe di neve sulle infrastrutture e costruzioni*. Presidenza del Consiglio dei ministri - Dipartimento per gli affari regionali e le autonomie.

Chiambretti, I. (2018). Neve, valanghe, fascino e rischio del "manto bianco": intervista a Igor Chiambretti, responsabile tecnico di Aineva. *CAE Magazine*, (20).

Christen, M., Bartelt, P., Bühler, Y., Deubelbeiss, Y., Salz, M., Schneider, M. e Schumacher, L. (2017). *RAMMS::DEBRISFLOW User Manual v1.7.0*.

Colbeck, S.C. (1982). An overview of seasonal snow metamorphism. *Rev. Geophys.*, 20(1), 45–61. DOI: https://doi.org/10.1029/RG020i001p00045

Erath, A. L. (2011). *Vulnerability assessment of road transport infrastructure* [Tesi di dottorato, ETH Zurich].

Frigo, B. (2003). *Effetti sulle strutture della componente aerosol delle valanghe di neve: il caso della Valle d'Aosta* [Tesi di Laurea]. Politecnico di Torino.

Frigo, Prola, Faletto (2012). *Valutazione della stabilità del manto nevoso: linee guida per la raccolta e l'interpretazione dei dati*, Regione Autonoma Valle d'Aosta.

Fusinaz, H. (2010). *Vulnerabilità delle costruzioni a rischio valanghe: applicazione ad un evento in Valle d'Aosta* [Tesi di laurea specialistica]. Politecnico di Torino, Torino, Italia.

Gauer, P. (2014). Comparison of avalanche front velocity measurements and implications for avalanche models. *Cold Regions Science and Technology*.

Gazzolo, T. (1963). Precipitazioni atmosferiche massime in n giorno avvenute in Italia nel quarantennio 1921-1960. In: *I Convegno Ing. Idraulici Corpo Genio Civile*, Parma, 1963.

Giani, G. (2014). Classificazione e tipologia delle valanghe di neve.

Jamieson, J.B. e Schweizer, J. (2000). Texture and strength changes of buried surface-hoar layers with implications for dry snow-slab avalanche release. *Journal of Glaciology*, 46(152), 151-160. DOI: https://doi.org/10.3189/172756500781833278

Jesenovec, S. (1995). *Pogubna razigranost: 110 let organiziranega hudourničarstva na Slovenskem: 1984-1994*. Ljubljana: PUH - Podjetje za urejanje hudournikov.

Kelly, D. e Staples, M. (2023). Radiation and Recrystallization: A Wasatch Avalanche Cycle. *International Snow Science Workshop 2023*, Bend, Oregon.

Komac, B. e Zorn, M. (2023). Impact of climate change on snowpack and avalanches in Slovenia: The Soča Valley case study. *Geographia Polonica*, 96, 29-51. DOI: https://doi.org/10.7163/GPol.0244

Komac, B., Ciglič, R., Hrvatin, M., Volk Bahun, M., Štaut, L. e Zorn, M. (2023). Geografski atlas naravnih nesreč v Sloveniji. *Geografski vestnik* 95-1. DOI: https://doi.org/10.3986/GV95105

Langham E. J. (1992) - Fisica e proprietà della neve. *Neve e Valanghe*, Aineva.

Leone, F., Colas, A., Garcin, Y., Eckert, N., Jomelli, V. and Gherardi, M. (2014). The snow avalanches risk on Alpine roads network. *Journal of Alpine Research | Revue de géographie alpine*, 102(4). DOI: https://doi.org/10.4000/rga.2501

Maggioni, M. in Gruber, U. (2003). The influence of topographic parameters on avalanche release dimension and frequency. *Cold Regions Science and Technology*.

Malešič, M. (2005): *Spomin in opomin gora. Kronika smrtnih nesreč v slovenskih gorah*. Didatka, Radovljica.

Martini, M. (2023). *Comparazione dei modelli di simulazione "FLO-2D" e "RAMMS::AVALANCHE" per la back-analysis di valanghe di neve* [Tesi di Laurea Magistrale, Università degli Studi di Padova].

McClung, D. e Schaerer, P. A. (2006). *The avalanche handbook*. The Mountaineers Books.

Meister, R. (1989). Influence of strong winds on snow distribution and avalanche activity. *Annals of Glaciology*.

Miller, T.R. (2000). Variations between countries in values of statistical life. *Journal of Transport and Policy*, 34(2).

Natek, K., Krevs, M., Lampič, B., Mrak, I., Ogrin, D., Repe, B. in Stepišnik, U. (2010). *Karte erozijske in poplavne nevarnosti, plazljivosti in nevarnosti snežnih plazov z aobmočje Občine Tržič*. Univerza v Ljubljani, Filozofska fakulteta. Ljubljana.

Nicolet, P., Jaboyedoff, M., Cloutier, C., Crosta, G. B. e Lévy, S. (2016). Brief communication: On direct impact probability of landslides on vehicles. *Nat. Hazards Earth Syst. Sci.*, 16, 995–1004.

Pagnutti D., Della Santa M. (2024), Valanga, lavina o slavina? Parole sotto la lente. *Vivere la Montagna*.

Praolini, A., Tognoni, G., Turroni, E., Valt, M., Filaferro, E., Lizzero, L., Del Barba, S., Valtolina, A., Barbolini, M. e Grafico, M. S. (2005). *Le valanghe*. AINEVA.

Rudolf-Miklau, F., Sauermoser, S. e Mears, A. I. (2015). *The Technical Avalanche Protection Handbook*. In *The Technical Avalanche Protection Handbook*. Wiley Blackwell.

Salm, B. (1993). Flow, flow transition and runout distances of flowing avalanches. *Annals of Glaciology*, 18, 221-226. DOI: https://doi.org/10.3189/S0260305500011551

Salm, B., Burkard, A. e Gubler, H. (1990). *Berechnung von Fliesslawinen, eine Anleitung fur Praktiker mit Beispielen*. Mitteilungen des Eidgenossischen Institutes fur Schnee und Lawinenforschung, No. 47, Davos, Switzerland.

Sauro, U. (2024). *Paesaggi della neve: un mondo da scoprire*. CAI Club Alpino Italiano.
Schweizer, J. (1999). Review of dry snow slab avalanche release. *Cold Regions Science and Technology*, 30(1–3), 43-57. DOI: https://doi.org/10.1016/S0165-232X(99)00025-7

Schweizer, J., J. B. Jamieson, and M. Schneebeli (2003), Snow avalanche formation, *Rev. Geophys.*, 41, 1016, doi:10.1029/2002RG000123, 4.

Tanabe, T., Tsunematsu, K. e Nishimura, K. (2025). Quantitative evaluation of probabilistic hazard mapping with polynomial chaos quadrature and its practical application. *Journal of Geophysical Research: Earth Surface*, 130, e2024JF007970. DOI: https://doi.org/10.1029/2024JF007970

Terzago, F. (2023). *Effetti delle valanghe di neve sulle infrastrutture energetiche* [Tesi di Laurea Magistrale, Politecnico di Torino].

THE WORLD BANK (2021). *Assessment of economic impacts from disasters along key corridors: Final report*.

Valt, M. (2016) Studio sulla relazione neve/pioggia nelle Alpi. Densità della neve fresca sulle Alpi Italiane. *Neve e Valanghe*, 87, 4.

Venturato, G. (2022). *Analisi di rischio valanghivo nel settore italiano del Monte Bianco (Val Ferret)* [Tesi di Laurea Magistrale, Politecnico di Torino].

Vigna, S. (2021). *Analisi di rischio da valanghe di neve in un comune in Valsesia* [Tesi di Laurea Magistrale, Politecnico di Torino].

Volk Bahun, M. (2020). *Mehanizmi Pojavljanja Snežnih Plazov V Slovenskih Alpah* [Tesi di

dottorato]. University of Primorska. Koper.

Wilhelm, C. (1997). Wirtschaftlichkeit im Lawinenschutz. Methodik und Erhebungen zur Beurteilung von Schutzmassnahmen mittels quantitativer Risikoanalyse und ökonomischer Bewertung. *Mitt. Eidg. Inst. Schnee- Lawinenforsch*.

WSL Istituto per lo studio della neve e delle valanghe SLF (2016): *Manuale dell'osservatore SLF*. Davos, WSL Istituto per lo studio della neve e delle valanghe SLF.

9. Acknowledgements

Desidero esprimere la mia più sincera gratitudine a tutti coloro che, in modi diversi, mi hanno supportato in questo percorso e hanno contribuito alla realizzazione di questa tesi.

In primo luogo, il mio più sentito ringraziamento va alla mia relatrice, Barbara Frigo, per la guida preziosa, la disponibilità e la presenza costante, che hanno reso possibile questo lavoro. Oltre al fondamentale supporto accademico, le sono particolarmente grato per aver assecondato il mio desiderio di svolgere questa tesi all'estero e per aver fatto tutto il possibile affinché questa esperienza si concretizzasse, nonostante le difficoltà iniziali.

Un ringraziamento speciale, anzi, un grazie gigante va a Blaž Komac, che mi ha accolto da subito con entusiasmo e mi ha dato l'opportunità di svolgere questa ricerca in un ambiente stimolante e altamente formativo, facendomi sentire davvero a casa. Il suo supporto è stato fondamentale sotto ogni aspetto, e gliene sarò sempre grato. Un grazie di cuore anche alla sua famiglia.

Non posso inoltre che ringraziare Marko, Lenart, Elizabeta, Miha e tutti i colleghi del Geografski inštitut Antona Melika - ZRC SAZU, che mi hanno coinvolto nella loro quotidianità, proponendomi esperienze arricchenti e accompagnandomi nella scoperta di un paese nuovo. Grazie a loro, questa esperienza è stata molto più di un semplice percorso accademico.

Un grazie di vero cuore alla mia famiglia: Angelica, Carlo, Noemi e Francesca. Grazie per esserci sempre, per il vostro sostegno incondizionato e per aver creduto in me anche quando io stesso vacillavo. Questo traguardo è vostro tanto quanto mio. Non servono altre parole, perché certe cose si sanno e basta.

Un enorme grazie va anche ai miei amici, quelli di sempre e quelli incontrati lungo il cammino. Nonostante i momenti complicati con l'università e le difficoltà che inevitabilmente hanno influenzato anche i rapporti umani, voi avete sempre remato nella mia stessa direzione, senza mai lasciarmi solo. Grazie per ogni chiacchierata, per ogni momento di leggerezza, per avermi sostenuto nei giorni difficili e festeggiato con me quelli belli. Siete fondamentali per me.

Infine, un grazie sincero a tutti coloro che, in un modo o nell'altro, hanno contribuito a questo lavoro con consigli, discussioni e supporto morale.

Grazie di cuore.

10. List of figures and tables